

SCIENTIFIC REPORTS



OPEN

A single molecule assay to probe monovalent and multivalent bonds between hyaluronan and its key leukocyte receptor CD44 under force

Received: 29 June 2016
Accepted: 08 September 2016
Published: 29 September 2016

Fouzia Bano¹, Suneale Banerji², Mark Howarth³, David G. Jackson² & Ralf P. Richter^{1,4,5}

Glycosaminoglycans (GAGs), a category of linear, anionic polysaccharides, are ubiquitous in the extracellular space, and important extrinsic regulators of cell function. Despite the recognized significance of mechanical stimuli in cellular communication, however, only few single molecule methods are currently available to study how monovalent and multivalent GAG-protein bonds respond to directed mechanical forces. Here, we have devised such a method, by combining purpose-designed surfaces that afford immobilization of GAGs and receptors at controlled nanoscale organizations with single molecule force spectroscopy (SMFS). We apply the method to study the interaction of the GAG polymer hyaluronan (HA) with CD44, its receptor in vascular endothelium. Individual bonds between HA and CD44 are remarkably resistant to rupture under force in comparison to their low binding affinity. Multiple bonds along a single HA chain rupture sequentially and independently under load. We also demonstrate how strong non-covalent bonds, which are versatile for controlled protein and GAG immobilization, can be effectively used as molecular anchors in SMFS. We thus establish a versatile method for analyzing the nanomechanics of GAG-protein interactions at the level of single GAG chains, which provides new molecular-level insight into the role of mechanical forces in the assembly and function of GAG-rich extracellular matrices.

Glycosaminoglycans (GAGs), a family of linear and anionic polysaccharides, are abundant in the extracellular space of vertebrates and act as vital regulators of the interactions between cells and their local environment. Simplest in structure among GAGs, hyaluronan (HA) is a regular polymer of disaccharides, composed of glucuronic acid and N-acetylglucosamine linked *via* alternating β -1,4 and β -1,3 glycosidic bonds, that can reach a contour length of several micrometers. The functional diversity of HA arises from its ability to bind various proteins, termed hyaladherins. These bind to the flexible HA chains and promote their self-assembly in hydrogel-like multimolecular complexes that frequently undergo further dynamic re-modelling. Such HA-rich matrices are of prime importance for regulating cell migration in key physiological processes such as inflammation¹ and fertilization², and in disease processes such as tumor metastasis³. HA also binds cell surface receptors, among which CD44 is structurally and biochemically the best characterized to date. In the vasculature, HA-CD44 interactions are known to mediate the recruitment of activated lymphocytes and neutrophils^{4,5} from the blood circulation, and have also been implicated in the recruitment of circulating stem cells⁶ and tumor cells^{7,8}.

Cells migrating within the extracellular matrix are profoundly affected by physical forces and the mechanical properties of their environment. This realization has driven efforts to probe and understand how forces act on the molecular scale⁹. A prime example is the capture of activated leukocytes from the blood flow during

¹CIC biomaGUNE, Paseo Miramon 182, 20009 Donostia-San Sebastian, Spain. ²MRC Human Immunology Unit, Weatherall Institute of Molecular Medicine, University of Oxford, Oxford, OX39DS, UK. ³Department of Biochemistry, University of Oxford, Oxford, OX13QU, UK. ⁴Université Grenoble Alpes - CNRS, Laboratoire Interdisciplinaire de Physique (LIPhy), BP 87, 38402 Saint Martin d'Hères, France. ⁵University of Leeds, School of Biomedical Sciences and School of Physics and Astronomy, Leeds, LS2 9JT, UK. Correspondence and requests for materials should be addressed to R.P.R. (email: rrichter@cicbiomagune.es)

inflammation, where mechanical forces are of vital importance in regulating adhesive interactions between PSGL-1 on the leukocyte surface and selectins on the blood vessel endothelium and the ensuing cell adhesion and rolling^{10,11}. In this particular scenario, interactions between HA and CD44 also experience the shear stress of the blood flow^{4,7,12}. More generally, given the structural role of GAG-protein interactions in the extracellular space, it is clear that these interactions are subjected to mechanical forces when matrix or tissues are deformed. To determine the biomechanical consequences of GAG-protein interactions, new methods are needed to probe the mechanical response of GAG-protein interactions at the nanoscale. On the most basic level, individual bonds need to be probed, and then, to better understand complexity in real biological systems, it must be determined how these elementary interactions are integrated into multivalent supramolecular systems. This is particularly important for GAGs because the polysaccharide chains can bind multiple proteins simultaneously.

Single molecule force spectroscopy (SMFS) is a powerful tool to study how forces affect molecular interactions, and to identify the underlying molecular mechanisms. In particular, atomic force microscopy (AFM) based SMFS is now well established for probing intra- and inter-molecular forces^{13–15}. A few SMFS studies have probed GAG-protein interactions on the single bond level^{16–19}, and similar assays have revealed specific and multivalent interactions between GAGs²⁰, or GAG analogues in the case of lower organisms²¹, on complex proteoglycans. To date however, only one study has applied SMFS to probe multivalent GAG-protein interactions¹⁷. Furthermore, these were not analysed in detail, and the particular assay system allowed only limited control over the orientation of the immobilized protein. Seminal studies (reviewed in ref. 22) with DNA, another biological polymer, not only demonstrate the unique ability of SMFS approaches to de-construct the dynamic and hierarchical assembly of large supramolecular complexes such as chromatin but they also highlight the critical importance of controlling the immobilization of such complexes for successful measurements. One of the main challenges to obtaining physiologically meaningful data using SMFS is achieving a well defined spatial arrangement of the studied molecules in their native orientation, while at the same time permitting the controlled application of the necessary tensile forces.

Here, we have devised such a method for GAG-protein interactions, by combining purpose-designed surfaces that afford immobilization of GAGs and receptors in the form of controlled nano-scale organizations with AFM SMFS. More specifically, the tailored surface functionalization and characterization by quartz crystal microbalance (QCM-D) and spectroscopic ellipsometry (SE) has enabled the anchoring of receptors and HA to solid substrates at controlled orientation, grafting density and lateral mobility. The new assay system has allowed us to study *monovalent* interactions between the leukocyte receptor CD44 and its HA ligand at the single molecule level as well as *multivalent* interactions between individual HA chains and CD44-coated surfaces in well-defined spatial arrangements. These measurements reveal that CD44-HA bonds have a high tensile strength despite their low affinity, and that multiple bonds along an HA chain rupture independently under load. We also demonstrate that strong but non-covalent bonds such as those between biotin and streptavidin (SAv), or between polyhistidine and metal chelators, which are ideal tools for immobilization of biomolecules at well-defined orientation and densities, are sufficiently strong to be used as anchors in the force spectroscopy of GAG-protein interactions. Our new method should thus be widely applicable to the study of GAG-protein interactions.

Results

In multivalent interactions, the (supra)molecular arrangement of the interaction partners can be critically important, and we therefore applied particular care in controlling the immobilization of both GAGs and proteins. Correct functionalization of surfaces with HA and its receptor CD44 was ascertained through quartz crystal microbalance (QCM-D) characterization.

Immobilization of HA. HA polymers of well-defined molecular mass (840 ± 60 kDa; contour length $2.10 \pm 0.15 \mu\text{m}^{23}$) were immobilized by end-grafting through a biotin tag at the reducing end. This method has been described previously^{24,25} and was applied here to AFM probes with incubation conditions adjusted such that only one or at most a few HA molecules are able to contact the protein-covered surface (Fig. 1a and Supplementary Fig. S1). In our force spectroscopy assays, polymeric HA fulfils three distinct functions. First, it serves as a flexible linker to discriminate specific interactions from undesired non-specific interactions that may occur when the AFM tip is close to the surface²⁶. Second, the HA polymer is long enough to accommodate several hundred HA-binding proteins simultaneously, and thus enables the study of both single bond and multivalent interactions between an individual HA chain and a protein-coated surface under load. The end-grafted HA chain transmits force to HA-receptor bonds in a well-defined and controlled way, thus facilitating quantitative data analysis.

Optimization of receptor immobilization procedures by QCM-D. The immobilization strategies for CD44 were devised to provide stable and specific immobilization at controlled orientation and lateral mobility, and at tunable surface densities. Specifically, the CD44 construct consisted of the extracellular domain (ECD) and a C-terminal His₁₀ tag for immobilization. CD44 was bound to either His-tag-capturing sensor surfaces *via* a Cu²⁺ chelate, or to supported lipid bilayers (SLBs) *via* a Ni²⁺-tris-nitilotriacetic acid (NTA) chelate²⁷, in a way that reproduces the native orientation of the HA binding domain on the plasma membrane (Fig. 1b).

QCM-D frequency and dissipation shifts (Δf and ΔD , respectively) upon exposure of CD44 to His-tag-capturing sensor surfaces showed saturable binding (Fig. 2), the magnitudes of which were consistent with the formation of a protein monolayer. Indeed, the frequency shift close to saturation ($\Delta f = -47 \pm 4$ Hz) corresponds to a film thickness of about 7 nm (see Methods), a value that is larger than the size of the HA binding domain alone (3.5 nm)^{28,29} and compatible with the estimated molecular mass (60 kDa) of the glycosylated CD44 domain (the exact dimensions of the full ECD are not known to our knowledge). CD44 remained stably bound throughout the buffer washing step, but was fully dissociated by elution with imidazole (Fig. 2a), confirming

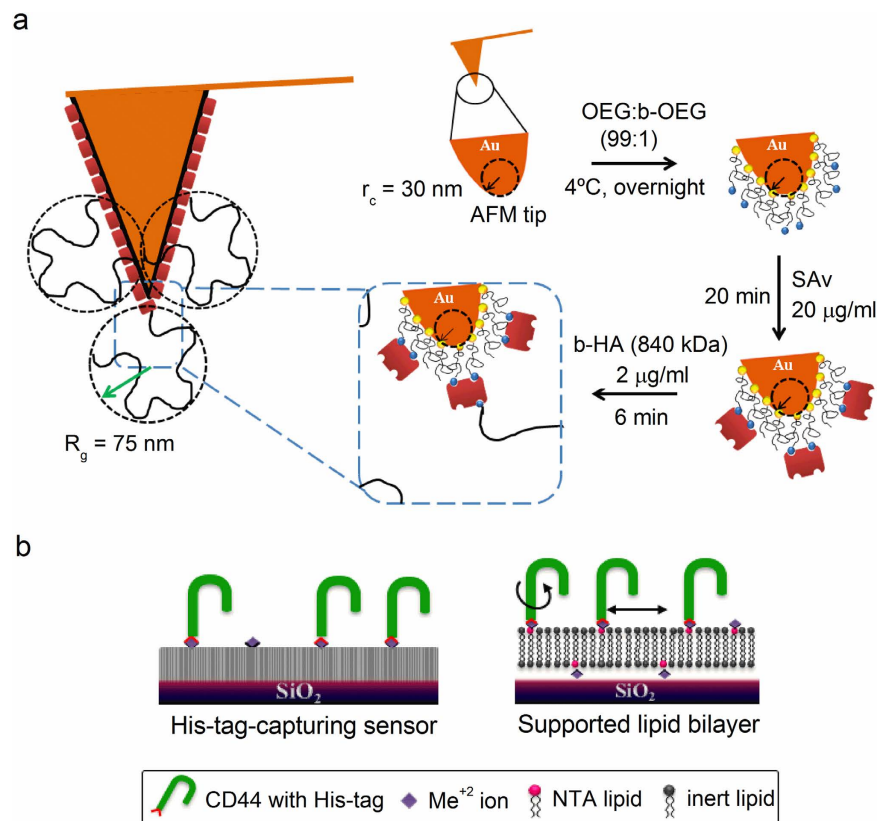


Figure 1. Surface functionalization with HA and CD44. (a) Representation (not to scale) of the protocol used to functionalize AFM probes with end-biotinylated HA (b-HA; 840 kDa) *via* monolayers of streptavidin (SAv) formed on a gold-supported mixed monolayer of thiolated oligo(ethylene glycol) with (b-OEG) and without (OEG) biotin. R_g is the radius of gyration of a single HA chain and r_c the radius of curvature of the apex of the AFM probe. (b) Representation of the architecture of surfaces (not to scale) displaying the cell-surface HA receptor CD44 either immobile (*i.e.*, His-tag-capturing layer; left) or laterally mobile (*i.e.*, SLB; right).

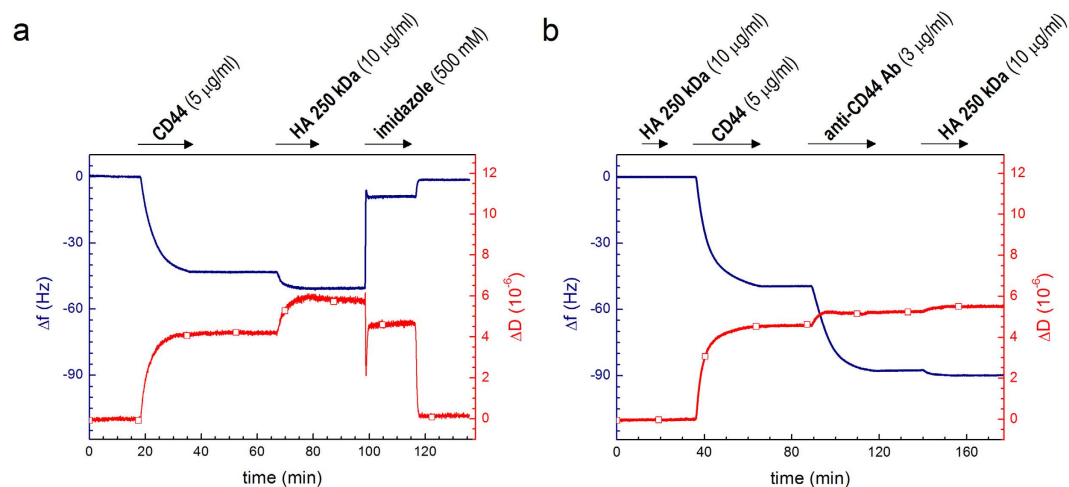


Figure 2. QCM-D immobilization assays for CD44 on His-tag-capturing sensors. QCM-D responses in (a) indicate formation of a stable and HA-binding CD44 monolayer, and demonstrate that CD44 is specifically immobilized through its polyhistidine tag (*i.e.*, it can be fully eluted in imidazole). Data in (b) demonstrate that HA binds through the authentic HA-binding site on CD44 (largely blocked with anti-CD44 Ab). The magnitude of the final shifts upon binding of HA polymer to CD44-coated surfaces were $\Delta f = -7.4 \pm 1.0$ Hz and $\Delta D = 1.7 \pm 0.2 \times 10^{-6}$.

its immobilization solely *via* the polyhistidine tag. HA polymers (250 kDa) adsorbed readily and stably to the immobilized CD44 monolayers (Fig. 2a; $\Delta f = -7.4 \pm 1.0$ Hz), whereas no binding was observed to bare sensors and only residual binding ($\Delta f = -2$ Hz) persisted when the HA-binding site of CD44 was impeded with the function-blocking anti-CD44 monoclonal antibody BRIC235³⁰ prior to HA incubation (Fig. 2b). The residual HA binding in this case most likely reflects incomplete blocking, *e.g.* due to spatial constraints of the large antibodies on the small receptor domains. These data clearly demonstrate that HA engages the authentic HA binding site on CD44. Given the low HA binding affinity for soluble CD44 as determined from previous surface plasmon resonance analyses ($K_D = 10$ to $100 \mu\text{M}$)³¹, the stable binding we observed to immobilized receptor most likely arises from multivalent ligand interactions³⁰.

Measurements of HA binding to CD44 immobilized on SLBs yielded similar results (Supplementary Fig. S2). Importantly, these SLBs retain the lateral mobility of CD44 in contrast to the conventional His-tag-capturing sensors in which the protein remains fixed³². In this way, the effect of receptor mobility on the interaction with HA can be independently assessed.

Immobilization of proteins for AFM SMFS. The immobilization procedures for CD44 established by QCM-D were then adopted to prepare samples for AFM SMFS. The solution concentration of CD44 was varied to generate surfaces with desired protein coverage, where the protein surface density was estimated from spectroscopic ellipsometry (SE) measurements and where we exploited the fact that the protein binding rate is largely mass transport limited (Supplementary Fig. S3). In the following, we operationally define root-mean-square (rms) distances between receptors around 50 nm (comparable to the size of the HA coil, $R_g \approx 75$ nm; Fig. 1) as 'low receptor density', and rms distances around 10 nm as 'high receptor density'.

We stress that the correct orientation of the immobilized proteins is critical for their functionality. For example, when another HA-binding protein, the aggrecan G1 domain complex with cartilage link protein³³ was immobilized through a randomly positioned tag, we detected only residual binding by QCM-D and AFM SMFS, revealing that only a very small fraction of the immobilized proteins engaged efficiently with HA (Supplementary Fig. S4).

Single molecule force spectroscopy of individual HA-CD44 bonds. We first used force spectroscopy to characterize the forces associated with the unbinding of HA from a single CD44 molecule (Fig. 3 and Supplementary Fig. S5). Predominantly single rupture events were observed when the HA-bearing AFM probe was exposed to His-tag-capturing surfaces with low CD44 density (rms distance ~ 50 nm; Fig. 3a). Several observations confirm that these curves indeed represent the genuine interaction of a single HA chain with a single CD44 molecule. First, most (78%) of the force curves ($n > 600$) showed no rupture event, and only a minor fraction (9%) showed two or more distinct rupture events: a distribution that would be predicted for stochastic single-molecule interactions. Second, the HA stretching curves in every case overlapped when the distances were normalized according to predictions of the worm-like chain (WLC) model (Supplementary Fig. S5a)³⁴. Third, no rupture events (in $n = 200$ force curves per condition) were observed when either CD44 or HA were omitted, indicating that the interactions are specific to these components (Supplementary Fig. S5b). Fourth, statistical analysis of force-separation curves with a single rupture event, acquired over a spectrum of retract velocities, using the WLC model revealed a velocity-independent persistence length ($L_p = 4.1 \pm 0.4$ nm; Fig. 3b). The magnitude of L_p agrees with previously reported values obtained from single-molecule HA stretching experiments at comparable ionic strength and pH values (4.4 ± 1.2 nm)³⁵. Fifth, the contour length L_c between the anchor point of HA and the CD44-binding locus varied broadly between measurements, and the maximum observed value matched the total contour length of the employed HA chains (2.1 μm) well (Fig. 3c). This confirms that a single HA chain is being stretched in our experiments and that CD44 can bind (with similar likelihood) at any position along that chain.

Histograms of the rupture forces revealed unimodal distributions for all retract velocities (Fig. 3d), suggesting that one specific bond is being probed. Indeed, the mean rupture force F depended linearly on the logarithm of the instantaneous loading rate r (Fig. 3e), as predicted by the Bell-Evans model^{13,36–38} for stochastic bond rupture under external load across a single energy barrier

$$F = \frac{k_B T}{x_\beta} \ln \left(\frac{r x_\beta}{k_{\text{off}} k_B T} \right), \quad (1)$$

where $k_B T$ is the thermal energy, x_β is the width of the energy barrier, and k_{off} is the unbinding rate constant in the absence of external load. Fitting of the data with Eq. (1) (Fig. 3e, line) yielded $k_{\text{off}} = 0.3 \pm 0.5 \text{ s}^{-1}$ and $x_\beta = 0.8 \pm 0.3$ nm.

We note that the above-mentioned minor fraction of force curves showing more than one rupture event (9%) might originate from the binding of an HA chain to several distinct CD44 molecules. Given the large size of HA, it is though also possible that rebinding to the same receptor molecule occurs during the retract phase. The dominance of force curves with single binding events over multiple binding events indicates that re-binding is a rare phenomenon under the experimental conditions.

Multivalent HA-CD44 interactions. Next, we used His-tag-capturing surfaces with high CD44 density (rms distance ~ 10 nm) to examine multivalent HA-receptor interactions. On these surfaces, force curves with a single rupture event were rare and multiple discrete unbinding peaks, typically around 10, were instead commonly observed (Fig. 4a,b).

The individual peaks in the force curves could be fitted closely (Fig. 4a) with a WLC model in which L_p was fixed to the previously established value of 4.1 nm. Detailed analysis over a spectrum of loading rates again

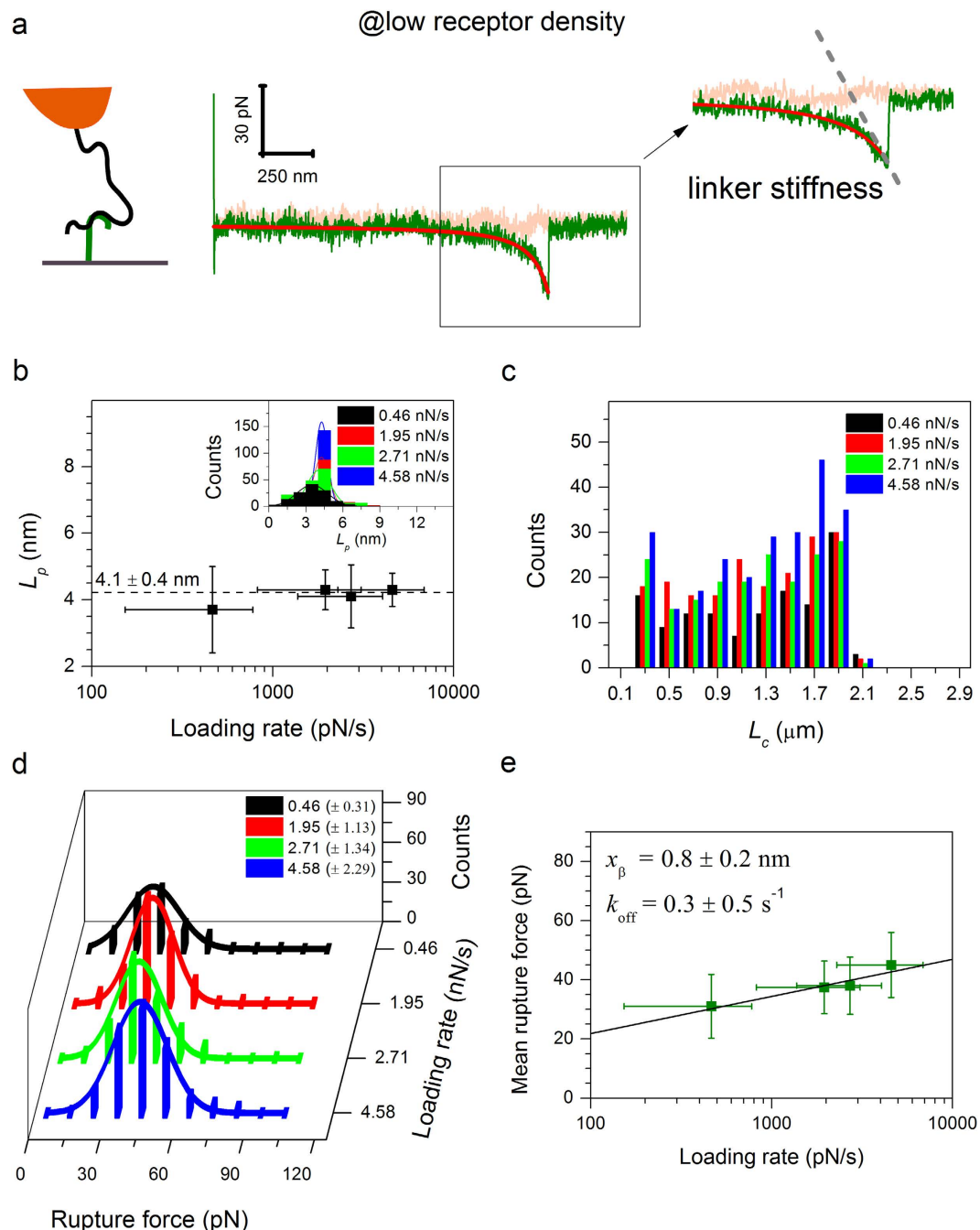


Figure 3. Analysis of HA-CD44 single-bond interactions. Representative force-separation curve (pink – approach, green – retract; retract velocity 1000 nm/s) recorded at low CD44 surface density (rms inter-CD44-distance ~ 50 nm) for a specific single unbinding event as schematically shown; the inset on the right shows an enlargement of the boxed portion of the force curve with an expanded separation axis. The red line represents a best-fit worm-like chain (WLC) model curve for HA stretching. The slope of this curve at the end of the extension curve (dashed line) corresponds to the linker stiffness and, together with the retraction speed, gives the instantaneous loading rate at the moment of bond rupture. **(b–e)** Results of the statistical analysis of single-rupture-event force curves, obtained at low CD44 density, with the WLC model. **(b)** Persistence length (L_p) of HA as a function of instantaneous loading rate. The dashed line marks the mean L_p value, with mean \pm s.d. indicated. The inset shows histograms of L_p for the studied instantaneous loading rates (as listed with color codes) with best-fit Gaussian curves. **(c)** Histograms of L_c , i.e. the contour length of the HA chain from its anchor point to the CD44 binding locus, for the studied instantaneous loading rates (as listed with color codes). The largest measured L_c is comparable to the total contour length of the employed HA chains ($2.1 \mu\text{m}$), as expected. **(d)** Rupture force histograms for the different instantaneous loading rates (listed in the back panel as mean \pm s. d.). The solid lines represent best-fit Gaussian curves. **(e)** Dynamic force spectra obtained from the data in **(d)**; error bars represent s.d. The black line represents the best-fit Bell-Evens model curve with kinetic parameters indicated.

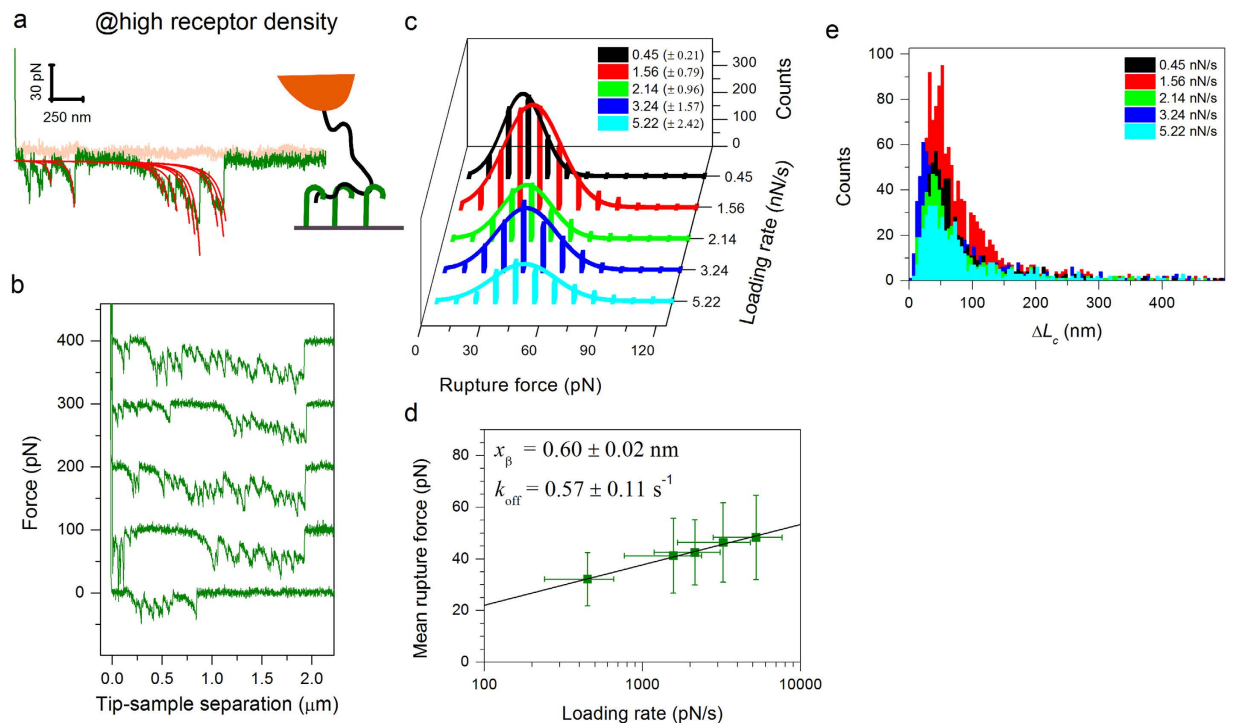


Figure 4. Analysis of HA-CD44 multivalent interactions. (a) Representative force-separation curve (pink – approach, green – retract; retract velocity 2000 nm/s) recorded at high CD44 surface density (rms inter-CD44-distance ~ 10 nm) for specific multiple unbinding events as schematically shown. The red lines represent best-fit WLC model curves ($L_p = 4.1$ nm fixed). (b) Five representative force-separation curves obtained under the same conditions; the curves are offset along the force axis for clarity. Each force curve is distinct, illustrating that bonds form stochastically at random positions along the HA chain. (c–e) Results of the statistical analysis of multiple-rupture-event force curves obtained at high CD44 density. (c) Rupture force histograms displayed analogous to Fig. 3d. (d) Dynamic force spectra displayed analogous to Fig. 3e. The similarity with the dynamic force spectra extracted from single-rupture-event curves (Fig. 3e) indicates that bonds rupture individually. (e) Histograms of HA loop length, equivalent to the contour length difference ΔL_c between successive rupture events.

revealed unimodal distributions of rupture forces (Fig. 4c), with distribution means and widths (Fig. 4d) that were fully consistent with the values obtained for interactions of an HA chain with a single CD44 molecule (Fig. 3e). The close match of the best-fit model curves with fixed L_p with the experimental data and the consistent distribution of rupture forces imply that all rupture events occur on the same HA chain, and that the individual bonds rupture independently from one another under load. The drastically enhanced number of rupture events at high CD44 surface density provided a larger dataset for statistical analysis (Fig. 4c) thus improving the accuracy of the determination of kinetic parameters through the Bell-Evans model (Fig. 4d): consolidated values were a barrier width $x_\beta = 0.60 \pm 0.02$ nm and a dissociation rate constant $k_{\text{off}} = 0.57 \pm 0.11$ s⁻¹.

From the sample force curves in Fig. 4a,b, it can be readily appreciated that the spacing between subsequent rupture events in a given force curve is irregular, and that the location of rupture events across different force curves varies widely. This indicates that HA interconnects CD44 molecules through loops of varying size, a picture that is consistent with simple theoretical predictions for the adsorption of flexible polymers to surfaces³⁹ and also with an earlier report on the thickness of films of HA polymers bound to CD44-coated surfaces³⁰. The difference in contour length between successive rupture events provides a measure for the contour length of a loop, and the histogram (Fig. 4e) revealed a broad distribution of loop sizes: the loop size distribution had a maximum around 50 nm, but loops of several 100 nm contour length could also be observed.

Role of lateral mobility in the rupture of HA-CD44 bonds. The experiments thus far assessed the behavior of immobilized CD44. However, under normal physiological conditions, HA receptors may be mobile in the cell membrane. To test how lateral mobility affects the unbinding of multivalent HA-receptor interactions, we performed complementary measurements with CD44 attached to SLBs. As shown in Fig. 5, the force curves and the distribution of rupture forces were comparable to those obtained on His-tag-capturing sensors (see *e.g.* Fig. 4), *i.e.* the receptor's lateral mobility does not substantially affect the unbinding process.

On the basis of all these findings, we conclude that individual HA-CD44 bonds are remarkably resistant to rupture under load considering their relatively low affinity, and that HA binds multivalently to a CD44-covered surface through the stochastic formation of loops, with bonds rupturing sequentially and independently under

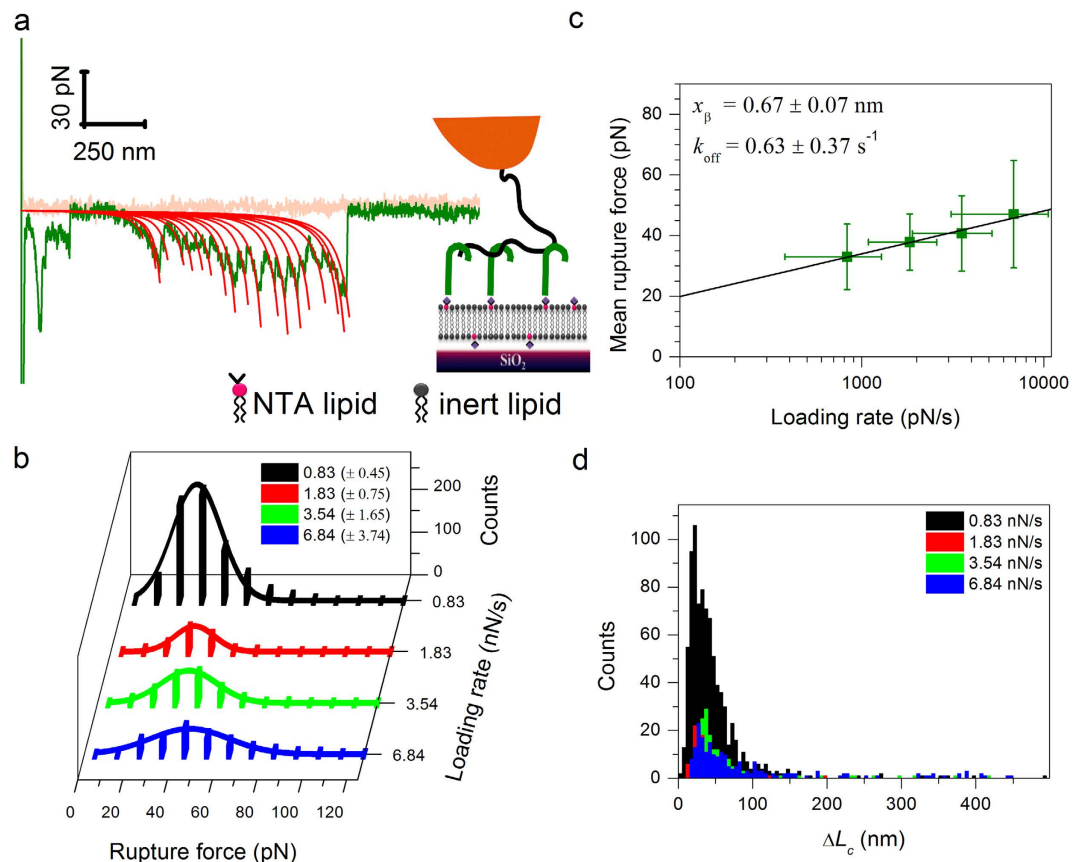


Figure 5. Effect of lateral mobility of CD44 on the interaction with HA. (a) Representative force-separation curve (approach/retract velocity 1000 nm/s) obtained between a HA-modified tip, and CD44 anchored to an SLB at high receptor density (rms inter-CD44-distance ~ 10 nm) as schematically shown (see also Supplementary Fig. S2). The force curve is qualitatively similar to those obtained for fully immobilized CD44 (cf. Fig. 4a,b). The red lines represent best-fit WLC model curves ($L_p = 4.1$ nm fixed). (b–d) Results of the statistical analysis of multiple-rupture-event force curves. (b) Rupture force histograms displayed analogous to Fig. 3d. (c) Dynamic force spectra displayed analogous to Fig. 3e. (d) Histograms of HA loop length, equivalent to the contour length difference ΔL_c between successive rupture events. These data are comparable to Fig. 4c–e, indicating that CD44 lateral mobility does not substantially affect the unbinding process.

load. In particular, these results illustrate that our approach is well suited for the characterization of monovalent and multivalent interactions with a single platform under well-defined interaction conditions.

Are CD44-HA bonds being probed? The rapid, strong and specific interactions between biotin and SAV, and between polyhistidine and metal chelators, are ideal for the anchorage of proteins and glycans at controlled orientation and density. Moreover, supported lipid bilayers with functionalized lipids being retained in the membrane through hydrophobic interactions are a unique platform to produce well-defined surfaces with laterally mobile receptors. However, given that these interactions are non-covalent, there is a finite possibility that an anchor point yields upon application of a tensile force, and it is thus *a priori* not clear if the above-determined parameters characterize the genuine HA-receptor interaction. To resolve this question, we performed a set of control experiments with distinct anchors.

First, we replaced streptavidin as an anchor for HA by traptavidin (TAv), a streptavidin variant that binds more stably to biotin (Supplementary Fig. S6)⁴⁰. The distributions of rupture forces with this modification were virtually identical compared to those obtained with SAV. Consequently, the kinetic parameters derived from the force spectra also agreed within experimental error (compare Supplementary Fig. S7c,d with Fig. 4c,d; Table 1). Moreover, single molecule force spectroscopy with biotin (attached to the AFM tip *via* a polyethylene glycol linker and a thiol-gold bond) and monolayers of SAV or TAv (prepared identically to the coatings used for HA attachment; Supplementary Figs S1 and S6) confirmed the enhanced mechanostability of TAv-biotin over SAV-biotin in our setup (Supplementary Fig. S8). Specifically, the mean rupture forces with TAv were increased by 10 to 20 pN compared to SAV within the range of loading rates tested (0.8 to 10 nN/s), and the derived kinetic parameters were comparable to those previously reported⁴⁰.

Second, we replaced the His-tag-capturing surface by a SAV monolayer for the anchorage of CD44 (Supplementary Fig. S9a–c). Our CD44 construct featured a biotin tag side by side with the polyhistidine tag at the C-terminus, and thus enabled the effect of the anchors to be compared at virtually identical protein

Anchor 1 ^a	Bond probed	Anchor 2 ^a	$k_{\text{off}}(\text{s}^{-1})$	$x_{\beta}(\text{nm})$	cf. Figure
Cu ²⁺ chelate-His ₁₀	CD44-HA	b-SAv-b ₂	0.57 ± 0.11	0.60 ± 0.02	4d
SLB-Ni ²⁺ chelate-His ₁₀		b-SAv-b ₂	0.63 ± 0.37	0.67 ± 0.07	5c
Cu ²⁺ chelate-His ₁₀		b-TAv-b ₂	0.44 ± 0.07	0.65 ± 0.02	S7d
b ₂ -SAv-b		b-SAv-b ₂	0.43 ± 0.21	0.65 ± 0.06	S9f
b ₂ -SAv	SAv-biotin	thiol-Au	1.40 ± 0.59	0.31 ± 0.03	S8f
b ₂ -TAv	TAv-biotin	thiol-Au	0.85 ± 0.58	0.28 ± 0.04	S8f

Table 1. Summary of kinetic parameters obtained from fitting force spectra with the Bell-Evans model.

^aAll non-covalent interactions in the chain of bonds are listed and indicated by “•”; biotin is abbreviated as “b”.

orientation on the surface. As for HA, the change in CD44 anchor had no substantial effect on the distribution of rupture forces and the derived kinetic parameters (compare Supplementary Fig. S9e,f with Fig. 4c,d; Table 1).

These control experiments demonstrate that the anchorages of HA *via* biotin and SAv, and of CD44 *via* polyhistidine and metal chelator, are strong enough and do not affect the force spectroscopy of HA-CD44 interactions appreciably. Moreover, the similar results obtained on SLBs (compare Fig. 5c,d with Fig. 4c,d; Table 1) imply that the anchorage of polyhistidine-binding lipids in the lipid bilayers is also strong enough. To explain this mechanistically, we performed in addition a theoretical analysis of rupture probabilities of bonds connected in series. We assumed that n bonds in a chain can rupture independently from each other, each according to the Bell-Evans model. Adopting the approach described by Neuert *et al.*⁴¹, the probability $\varphi^{(i)}$ of bond i to rupture as a function of force f and loading rate r is defined by a system of $n + 1$ coupled ordinary differential equations

$$\frac{d\varphi^{(i)}(f, r)}{df} = \varphi^{(i)}(f, r) \frac{k_{\text{off}}^{(i)} \exp\left(\frac{fx_{\beta}^{(i)}}{k_B T}\right)}{r} \quad \text{and} \quad \frac{d\Phi(f, r)}{df} = -\Phi(f, r) \sum_{i=1}^n \frac{k_{\text{off}}^{(i)} \exp\left(\frac{fx_{\beta}^{(i)}}{k_B T}\right)}{r}, \quad (2)$$

where $\Phi = 1 - \sum_{i=1}^n \varphi^{(i)}$ is the probability of the n -bond chain to remain intact. The boundary conditions to solve these equations are defined by the n -bond chain being intact at the start of the measurement ($\Phi = 1$ and $\varphi^{(i)} = 0$ at $f=0$).

To compare with our experiments, we considered for simplicity a system with two reversible bonds, representing CD44-HA and a SAv-biotin anchorage (thus effectively assuming the second anchorage to be irreversible). For SAv-biotin, we used the experimentally determined values for k_{off} and x_{β} (Supplementary Fig. S8f; Table 1) as input parameters. For CD44-HA, we used the values shown in Fig. 4d (and Table 1), as our control experiments had shown that these represent the individual CD44-HA interaction adequately even though they were obtained in a system with multiple bonds in series.

Figure 6a shows the results of the numerical calculations in the form of the derivative $d\varphi/df$ of the rupture probability as a function of the force f at two selected loading rates (1 and 10 nN/s) that are close to the lowest and highest loading rates used experimentally, respectively. This plot reveals that the breakage of CD44-HA dominates over SAv-biotin, but also that the probability of SAv-biotin to break is sizeable.

Figure 6b shows the rupture probability φ of the individual bonds in the limit of high forces when all chains have effectively ruptured ($\Phi = 0$). This plot illustrates that the rupture of CD44-HA dominates over SAv-biotin over the entire range of experimental loading rates. The probability of the anchor to rupture is though sizeable (between 10 and 30%), and is reduced by approximately two-fold when SAv-biotin is replaced by the more stable TAv-biotin.

Figure 6c compares the numerical calculations for the total rupture probability of the two bonds in series (*i.e.* cumulating the ruptures of either CD44-HA or SAv-biotin) with the expected response for scenarios in which there is only one reversible bond, *i.e.* either CD44-HA or SAv-biotin (for $n = 1$, Eq. (2) simplifies to $d\varphi/df = \varphi k_{\text{off}} \exp[fx_{\beta}/(k_B T)]/r$). From this presentation, it can be appreciated that the curves for CD44-HA alone are very similar to the curves for the two bonds in series, to such an extent that the width and the mean of the distribution are barely affected by the presence of the SAv-biotin bond. Specifically, the decrease in the location of the maxima in the distributions owing to the presence of SAv-biotin remained within ~ 1 pN. This is below the resolution limit of our experiments, and explains that the occasional breakage of SAv-biotin, when in series with CD44-HA, does not affect the force spectra appreciably that are ultimately used for fitting with the Bell-Evans model (Eq. (1)).

We note that the presentation in Fig. 6c is equivalent to idealized rupture force histograms. The mean rupture forces predicted for CD44-HA alone and SAv-biotin alone are in agreement with the experimental data in Fig. 4d and Supplementary Fig. 8f, respectively. This is to be expected because these data were effectively used as input parameters, and merely confirms that the numerical calculations are correct. Reassuringly, however, the widths of the distributions in Fig. 6c also compare well with the experimental data (*cf.* standard deviations indicated in Fig. 4d and Supplementary Fig. 8f). The width was not an input parameter of the numerical calculations, and the agreement thus provides further support for the validity of the simple theoretical model described by Eq. (2).

Collectively, the experimental results at low and high receptor density demonstrate that the stochastic rupture of individual bonds between HA and CD44 can be reliably characterized in our experimental setup, thus validating that the kinetic parameters shown in Figs 4d and 5c pertain to the genuine interaction of HA with its receptor. The results of the theoretical model are fully consistent with our experimental findings and confirm

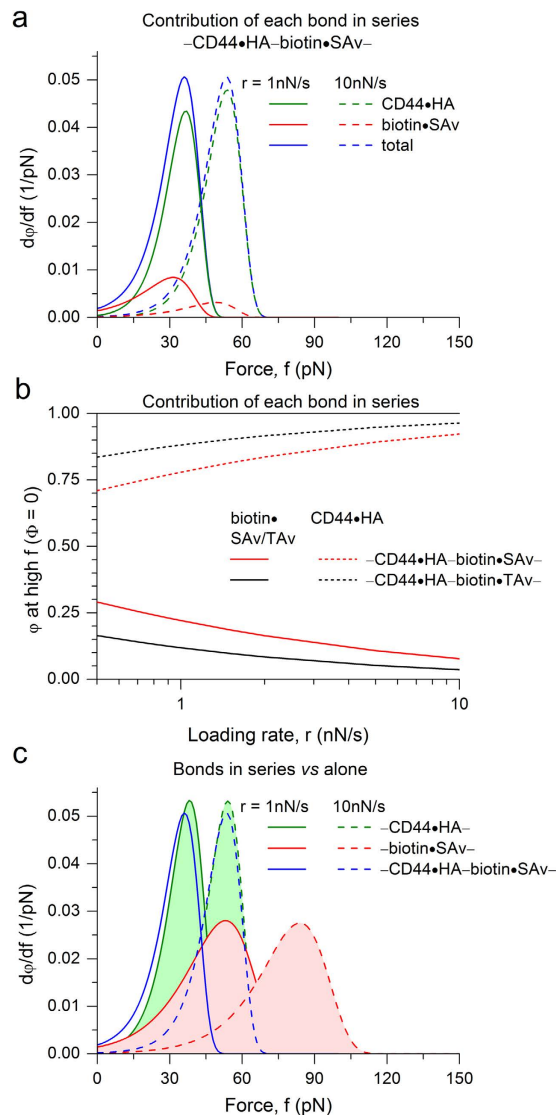


Figure 6. Theoretically predicted rupture probabilities for two reversible bonds in series. (a) Derivative of the rupture probability $d\phi/df$ vs. force f for the scenario of CD44-HA in series with SAV-biotin at loading rates $r = 1$ nN/s (solid lines) and 10 nN/s (dashed lines); data for $\phi^{(\text{CD44-HA})}$ is shown in green, for $\phi^{(\text{SAv-biotin})}$ in red, and for the total rupture probability $\phi^{(\text{total})} = \phi^{(\text{CD44-HA})} + \phi^{(\text{SAv-biotin})}$ in blue. (b) Rupture probabilities ϕ in the limit of high forces ($\Phi = 0$) vs. loading rate r for the scenarios of CD44-HA in series with SAV-biotin (red) or TAV-biotin (black); $\phi^{(\text{CD44-HA})}$ is shown as solid lines, $\phi^{(\text{SAv-biotin})}$ and $\phi^{(\text{TAv-biotin})}$ as dashed lines. The rupture of CD44-HA dominates over SAV-biotin over the entire range of loading rates, and the probability of the anchor to rupture is reduced by approximately two-fold upon replacing SAV-biotin by TAV-biotin. (c) Total rupture probabilities, displayed as $d\phi/df$ vs. force f , for the scenario of CD44-HA in series with SAV-biotin (as shown in (a); blue lines) compared to CD44-HA alone (light green filling), and SAV-biotin alone (light red filling). The curves for CD44-HA alone are very similar to the curves for the two bonds in series, demonstrating that the occasional breakage of SAV-biotin, when in series with CD44-HA, does not affect the force spectra appreciably. See Table 1 and main text for the input data of the theoretical model.

that the anchors break occasionally but are mostly stable and sufficiently strong not to perturb the analysis of the HA-CD44 interaction with the Bell-Evans model.

Discussion

In this manuscript we have conceived an experimental platform for the analysis of the nanomechanics of GAG-protein interactions. Focusing on the fundamentally important interaction between HA and its primary cell surface receptor CD44, we have demonstrated how GAG-protein binding can be analyzed at the level of a single GAG chain in a well-defined system that not only preserves the native orientation of the receptor, but which also enables important parameters such as its density and lateral mobility in the membrane to be varied. With this system, the unbinding mechanics of monovalent and multivalent GAG-protein interactions can be measured and directly compared.

HA-CD44 interactions are critical for capturing circulating cells such as activated lymphocytes and neutrophils from the blood flow⁵, enabling their transient adhesion to the luminal surface of the vessel, and the characteristic rolling behavior that precedes extravasation^{4,7,12,42,43}. Among studies on the interaction of HA with CD44 on a larger scale (involving many HA chains)^{7,12,44}, binding of CD44-positive cells and CD44-coated microspheres to HA-coated surfaces has been reported to strengthen under flow, and it has been proposed that this effect is encoded at the molecular level in the form of an unconventional bond that strengthens under force (catch bond)^{7,12}. In the measurements described here, the dependence of the mean rupture force on loading rate as well as the magnitude of the standard deviations in mean rupture force (Figs 3e and 4d) are consistent with the predictions of the Bell-Evans model indicating that CD44-HA bond rupture is adequately described by conventional unbinding across a single barrier. These two scenarios, however, are not mutually exclusive: as recently demonstrated by Harder *et al.*¹⁹ for a different GAG-protein bond, the catch bond behavior may simply not be picked up over the range of loading rates accessible in our experiments. This question clearly deserves further study in the future. On the multi-bond level, the major finding of this study is that multiple CD44-HA bonds along a single HA chain rupture sequentially and independently under load (Fig. 4). Leukocyte rolling along the luminal surface of blood vessels mediated by CD44-HA interactions would thus rely largely on the stochastic rupture and renewal of CD44-HA bonds.

Raman *et al.*¹⁶ have previously reported single molecule force data on CD44-HA bonds, and it is notable that the mean rupture forces reported with their assay exceed those measured here by about two-fold. The presentation of HA in the earlier work was distinct, with HA polymers being chemically modified at multiple sites along the polymer chain, likely resulting in multiple attachment points to the AFM tip. Furthermore, the CD44 constructs employed and their anchorage to the surface were also different to those in our study. A definitive explanation at this stage is difficult, however, because representative force-separation curves or force histograms were not provided in the earlier study and hence cannot be compared directly with the data presented here.

We have here studied the interaction of HA with a selected construct of CD44. The binding of HA to CD44 on the cell surface in the absence of tensile force has previously been found to be tightly regulated through CD44 post-translational modifications, such as N-glycosylation and terminal sialylation⁴⁵ and receptor clustering. Future studies should focus on the possible contributions of such modifications to the regulation of HA binding under force. In addition, it will also be interesting to compare the mechanical response of CD44-HA bonds with the bonds that HA forms with other cell surface receptors such as the lymphatic vessel endothelial receptor-1 (LYVE1)^{46–48}. Such a comparison would be of particular interest, as the lymphatic system experiences lower flow and shear stress than the blood vasculature and how the two receptors respond to the distinct mechanical environments in which they act remains an open question.

Our methodology for protein and GAG immobilization relies on the bio-affinity of selected tags, a feature which offers rapid assembly and precise control on molecular orientations. With its modular design, and the increasing availability of methods for the site-specific tagging of proteins and GAGs⁴⁹ with polyhistidine or biotin, the platform can now be readily applied to a wide range of different proteins and their GAG ligands. Several extensions of the assay platform are conceivable. First, future progress in the conjugation of GAGs may enable the effects of their disposition to be tested through selective tethering *via* the reducing or non-reducing ends as well as permitting analysis of the effects of GAG topology (*e.g.* GAGs containing loops of defined size) on the mechanical response. Second, other force spectroscopy schemes such as force clamps or variations in the direction of applied force could provide further insight into bond mechanics to resolve the presence of multiple unbinding pathways underlying unconventional behavior such as catch bonds¹⁹, and their effect on multivalent interactions. In this regard, the method should also be applicable to other single-molecule techniques that require immobilization of the interaction partners on surfaces, such as magnetic tweezers, laminar flow assays, acoustic force spectroscopy, or centrifuge force microscopy (see ref. 50 and references therein). Third, other aspects of the *in vivo* conditions also can be readily incorporated to probe the regulatory role of multiple simultaneous protein-GAG interactions. For example, experiments in which GAG-binding proteins are presented in the solution phase jointly with the immobilized receptors would help determine how the modulation of GAG structure by proteins⁵¹, such as that of HA by TSG-6⁵², affects the nanomechanics of GAG binding to the cell surface. Last but not least, our methodology could conceivably be combined with the analysis of GAG-receptor interactions in live cells. This would enable a direct comparison of responses in biomimetic systems that are well defined and recapitulate selected properties of the cell surface with the more complex (and less well defined) native system.

The ideal anchorage of biomolecules in SMFS is both well defined (in terms of orientation, surface density and lateral mobility) and resistant to tensile force. In practice this represents a trade-off scenario: covalent attachment guarantees high mechanical strength but is often not well defined, whereas attachment through bio-affinity tags is very well defined but the resistance to tensile force is lower. In this regard, the combination of adequately designed control experiments with a simple theoretical model (Eq. (2)) provides an effective tool to assess the viability of non-covalent bonds as anchors in SMFS. Our results demonstrate that interactions of biotin with SAv, and polyhistidine with metal chelators, and the embedding of metal-chelator functionalized lipids in lipid bilayers, are sufficiently strong for the reliable analysis of HA-CD44 interactions. Given the relatively weak nature of typical GAG-protein interactions, it is likely that the anchor stability will also be sufficient to study many other interactions. Where needed, the accessible force range can be extended by the use of TAv instead of SAv. Moreover, the model presented in Eq. (2) may also be used to correct for the effect of anchors in cases where the rupture probability of anchor(s) is comparable to that of GAG-protein interactions, thus further extending the application range. To this end, a data fitting procedure can be envisaged that uses k_{off} and x_0 of the anchor bonds (determined with control measurements for each anchor type; *cf.* Fig. S8) as input to extract the k_{off} and x_0 values for the GAG-protein interaction from experimental force spectra for the GAG-protein bond in series with the anchor bonds. The sensitivity of the assay to the GAG-protein bond (and thus the accuracy of the correction method)

can be expected to be good as long as the rupture probability of the GAG-protein bond is larger than that of the anchors, but to decrease rapidly in the inverse case.

In summary, we have reported the combination of tailored surface functionalization strategies and surface characterization by QCM-D and SE with AFM SMFS to study the nanoscale mechanics of monovalent and multivalent bonds between proteins and GAGs at a level down to a single GAG chain in supramolecular architectures that are designed to reproduce specific aspects of the *in vivo* situation. Applying this approach, we have quantified the mechanical strength of individual CD44-HA bonds and revealed that multiple bonds along a given HA chain rupture sequentially and independently under load. This platform technology should be widely applicable for elucidating molecular mechanisms underlying the response of extracellular matrix and cell surface receptors to mechanical forces.

Methods

Buffer, proteins and hyaluronan. A ‘working’ buffer consisting of 10 mM HEPES at pH 7.4 and 150 mM NaCl was used to dilute proteins and HA and throughout all QCM-D and AFM experiments. The full-length ECD (terminating after residue number 267) of human CD44 with a His₁₀ tag and a biotin tag at the C-terminus was produced and purified as described in the Supplementary Methods. Monoclonal mouse anti-human CD44 function-blocking antibody BRIC235 (anti-CD44 Ab) was obtained from International Blood Group Reference Laboratory (Bristol, UK). Lyophilized SA_v (Sigma Aldrich) was dissolved in ultrapure water to form a stock at 1 mg/ml concentration. TA_v was expressed and purified from *E. coli* as described previously⁴⁰, stored at 1 mg/ml in PBS at –20 °C, and further diluted in working buffer for final use. Lyophilized HA polymers with well-defined molecular masses (SelectHA) were purchased from Hyalose (Oklahoma City, OK, USA): HA with a biotin at its reducing end (for AFM SMFS assays) had a molecular mass of 840 ± 60 kDa, and plain HA (for QCM-D assays) had a molecular mass of 250 ± 12 kDa. HA was dissolved, and gently shaken for 2 h in ultrapure water, to provide a stock of 1 mg/ml. Stock solutions of all proteins and HA were aliquoted and stored at –20 °C. Thawed aliquots of proteins were used within a few days, while thawed aliquots of HA were used within a few weeks.

Lipids. 1,2-dioleoyl-sn-glycero-3-phosphocholine (DOPC) was purchased from Avanti Polar Lipids (Alabaster, AL, USA). Tris-NTA-functionalized lipid analogues ((NTA)₃-SOA)⁵³, prepared as previously described⁵⁴ were kindly provided by J. Piehler (Osnabrück University, Germany). Small unilamellar vesicles (SUVs) in working buffer were prepared by sonication from a mixture of DOPC and (NTA)₃-SOA (95:5 molar ratio), as described previously^{55,56}. SUVs at a stock concentration of 1 to 2 mg/ml were stored at 4 °C under argon and used within three weeks.

Substrates. QCM-D sensors with gold coating (QSX301), silica coating (QSX303) and His-tag-capturing coating (QSX340) were obtained from Biolin Scientific (Västra Frölunda, Sweden). Silicon wafers (9 mm × 9 mm) with a native oxide layer of about 2 nm were from University Wafers (South Boston, MA, USA). 100 nm gold coatings were prepared by sputter deposition.

Silica-coated substrates were cleaned with 2% (w/v) SDS for 30 min, rinsed thoroughly with ultrapure water followed by blow-drying with N₂, and treated with UV/ozone (Bioforce Nanoscience, Ames, IA) for 30 min and stored in air. His-tag-capturing sensors were used as received and regenerated by 5 mM CuSO₄. Gold-coated substrates were employed as received and not re-used.

Surface functionalization. *Preparation of surfaces for anchorage of biotin-tagged hyaluronan and proteins.* Di-end functional oligo(ethylene glycols) (OEGs) were purchased from Polypure (Oslo, Norway), one made of two EG₇ with hydroxyl groups on one end and connected by a disulfide on the other (OEG disulfide), and the other containing EG₁₀ with biotin on one end and a thiol on the other (b-OEG thiol). Gold-coated planar substrates or AFM cantilevers were conditioned by exposure to UV/ozone for 30 min, and then immersed overnight at 4 °C in an ethanolic solution (purity 99.9%; Scharlab S.L.) of OEG disulfide and b-OEG thiol (molar ratio 500:1) at a total concentration of 1 mM. Prior to use, the functionalized substrates were rinsed with ethanol and blow-dried with N₂. This procedure provides a monolayer of OEG that is inert to non-specific binding of proteins and GAGs; it permits the formation of a monolayer of SA_v that serves as a ‘molecular breadboard’ for the controlled anchorage of biotin-tagged molecules^{24,25}.

Preparation of surfaces for anchorage of polyhistidine tagged proteins. His₁₀-tagged CD44 was directly immobilized on His-tag-capturing QCM-D sensors. This sensor surface features a passivating layer of poly(ethylene glycol) (PEG) and exposes divalent metal ions for capturing polyhistidine tagged molecules. Alternatively, SLBs containing Ni²⁺-loaded tris-NTA moieties were used to anchor polyhistidine tagged proteins. To this end, silica-coated substrates were conditioned by exposure to UV/ozone for 30 min prior to use, and SLBs were formed from SUVs by the method of vesicle spreading, as described previously⁵⁷.

For anchorage of HA and proteins, the surfaces were incubated with the appropriate molecule (biotin or His tagged) at ambient conditions in working buffer at the required concentration. To obtain receptor monolayers of ‘low’ (~0.07 pmol/cm²) and ‘high’ (~1.8 pmol/cm²; Supplementary Fig. S3) density, respectively, CD44 was incubated in still solution for 30 min at 0.25 µg/ml and 6.5 µg/ml.

Quartz crystal microbalance (QCM-D). QCM-D measures the changes in resonance frequency, Δf , and dissipation, ΔD , of a sensor crystal upon molecular adsorption on its surface. The QCM-D response is sensitive to the areal mass density (including hydrodynamically coupled water) and the mechanical properties of the surface-bound layer. To a first approximation, a decrease in frequency (Δf) corresponds to increased mass, while a low (high) response in dissipation (ΔD) corresponds to rigid (soft) films. QCM-D measurements were carried out with a Q-Sense E4 system equipped with Flow Modules (Biolin Scientific AB, Västra Frölunda, Sweden) with flow

rates of 5 to 20 $\mu\text{m}/\text{min}$ at a working temperature of 23 °C. Δf and ΔD were collected at six overtones ($i = 3, 5, 7, 9, 11, 13$). Changes in dissipation, ΔD , and normalized frequencies, $\Delta f = \Delta f_i/i$, for $i = 3$ are presented. All overtones provided similar information. All experiments were carried out in duplicate; numbers in the manuscript text represent the mean \pm variations around the mean.

For dense monolayers of globular proteins, the film thickness was estimated from $d = -C/\rho \times \Delta f$, where the density $\rho = 1.2 \text{ g}/\text{cm}^3$ represents the protein film density to within an error of less than 20% and $C = 18.1 \text{ ng}/\text{cm}^2/\text{Hz}$ the sensor's mass sensitivity constant⁵⁸.

Force spectroscopy. AFM experiments were performed on a NanoWizard II system (JPK, Berlin, Germany) in working buffer at ambient conditions, using gold-coated cantilevers with nominal spring constants of 30 or 6 pN/nm (Biolevers), and 60 pN/nm (NPG-10; both from Bruker AFM Probes, USA). The real spring constants were determined by the thermal noise method⁵⁹. Force curves were acquired at selected approach and retract velocities with a maximal applied load of 600 pN and minimal surface dwell time (*i.e.* 0 ms), except otherwise stated. For a given set of AFM probe, surface and interaction settings, several hundreds to thousands of individual force curves were acquired to sample stochastic variations in the interactions. All experiments were performed at least twice with distinct yet identically prepared AFM probes and surfaces.

Force curves were analyzed with JPK data processing software. For quantitative analysis of the stretching of individual HA chains and to extract HA-CD44 bond rupture forces, force-separation curves were fitted to the WLC model⁶⁰. Unless otherwise stated, both persistence length and contour length were adjustable parameters, and only rupture events occurring at tip-sample distances larger than 200 nm were considered, to avoid bias by non-specific tip-sample interactions. Instantaneous loading rates r were computed from the effective spring constant k_{eff} , corresponding to the slope of the WLC best-fit curve close to the rupture (Fig. 3a, inset), and the retract velocity v as $r = k_{\text{eff}}v$. The kinetic parameters k_{off} and x_{β} were determined by non-linear regression analysis with OriginPro software (OriginLab, Northampton, MA) of mean rupture force vs. instantaneous loading rate data with the Bell-Evans model^{13,38}, where the standard error of the mean rupture force was considered to compute confidence intervals for the kinetic parameters.

References

- Day, A. J. & de la Motte, C. A. Hyaluronan cross-linking: a protective mechanism in inflammation? *Trends Immunol.* **26**, 637–643 (2005).
- Russell, D. L. & Salustri, A. Extracellular matrix of the cumulus-oocyte complex. *Semin. Reprod. Med.* **24**, 217–227 (2006).
- Toole, B. P. Hyaluronan: from extracellular glue to pericellular cue. *Nat. Rev. Cancer* **4**, 528–539 (2004).
- Mohamadzadeh, M., DeGrendele, H., Arizpe, H., Estess, P. & Siegelman, M. Proinflammatory stimuli regulate endothelial hyaluronan expression and CD44/HA-dependent primary adhesion. *J. Clin. Invest.* **101**, 97–108 (1998).
- McDonald, B. & Kubes, P. Interactions between CD44 and Hyaluronan in Leukocyte Trafficking. *Front. Immunol.* **6**, 68 (2015).
- Avigdor, A. *et al.* CD44 and hyaluronic acid cooperate with SDF-1 in the trafficking of human CD34+ stem/progenitor cells to bone marrow. *Blood* **103**, 2981–2989 (2004).
- Christophis, C. *et al.* Shear stress regulates adhesion and rolling of CD44+ leukemic and hematopoietic progenitor cells on hyaluronan. *Biophys. J.* **101**, 585–593 (2011).
- Richter, U., Wicklein, D., Geleff, S. & Schumacher, U. The interaction between CD44 on tumour cells and hyaluronan under physiologic flow conditions: implications for metastasis formation. *Histochem. Cell Biol.* **137**, 687–695 (2012).
- Hoffman, B. D. & Crocker, J. C. Cell mechanics: dissecting the physical responses of cells to force. *Annu. Rev. Biomed. Eng.* **11**, 259–288 (2009).
- Fritz, J., Katopodis, A. G., Kolbinger, F. & Anselmetti, D. Force-mediated kinetics of single P-selectin/ligand complexes observed by atomic force microscopy. *Proc. Natl. Acad. Sci. USA* **95**, 12283–12288 (1998).
- Evans, E., Leung, A., Hammer, D. & Simon, S. Chemically distinct transition states govern rapid dissociation of single L-selectin bonds under force. *Proc. Natl. Acad. Sci. USA* **98**, 3784–3789 (2001).
- Suzuki, T. *et al.* Mechanical force effect on the two-state equilibrium of the hyaluronan-binding domain of CD44 in cell rolling. *Proc. Natl. Acad. Sci. USA* **112**, 6991–6996 (2015).
- Evans, E. Probing the relation between force–lifetime–and chemistry in single molecular bonds. *Annu. Rev. Biophys. Biomol. Struct.* **30**, 105–128 (2001).
- Ott, W., Jobst, M. A., Schoeler, C., Gaub, H. E. & Nash, M. A. Single-molecule force spectroscopy on polyproteins and receptor-ligand complexes: The current toolbox. *J. Struct. Biol.* (2016) *In Press*.
- Scholl, Z. N., Li, Q. & Marszalek, P. E. Single molecule mechanical manipulation for studying biological properties of proteins, DNA, and sugars. *WIREs Nanomed. Nanobiotechnol.* **6**, 211–229 (2014).
- Raman, Phrabha S., Alves, Christina S., Wirtz, D. & Konstantopoulos, K. Distinct Kinetic and Molecular Requirements Govern CD44 Binding to Hyaluronan versus Fibrin(ogen). *Biophys. J.* **103**, 415–423 (2012).
- Milz, F. *et al.* Cooperation of binding sites at the hydrophilic domain of cell-surface sulfatase Sulfl allows for dynamic interaction of the enzyme with its substrate heparan sulfate. *Biochim. Biophys. Acta* **1830**, 5287–5298 (2013).
- Liu, X., Sun, J. Q., Heggeness, M. H., Yeh, M. L. & Luo, Z. P. Force-mediated dissociation of proteoglycan aggregate in articular cartilage. *Biorheology* **43**, 183–190 (2006).
- Harder, A. *et al.* Catch Bond Interaction between Cell-Surface Sulfatase Sulfl and Glycosaminoglycans. *Biophys. J.* **108**, 1709–1717 (2015).
- Harder, A., Walhorn, V., Dierks, T., Fernandez-Busquets, X. & Anselmetti, D. Single-molecule force spectroscopy of cartilage aggregate self-adhesion. *Biophys. J.* **99**, 3498–3504 (2010).
- Garcia-Manyes, S. *et al.* Proteoglycan mechanics studied by single-molecule force spectroscopy of allotypic cell adhesion glycans. *J. Biol. Chem.* **281**, 5992–5999 (2006).
- Chien, F. T. & van Noort, J. 10 years of tension on chromatin: results from single molecule force spectroscopy. *Curr. Pharm. Biotechnol.* **10**, 474–485 (2009).
- Almond, A., Brass, A. & Sheehan, J. K. Oligosaccharides as Model Systems for Understanding Water–Biopolymer Interaction: Hydrated Dynamics of a Hyaluronan Decamer. *J. Phys. Chem. B* **104**, 5634–5640 (2000).
- Baranova, N. S. *et al.* The inflammation-associated protein TSG-6 cross-links hyaluronan via hyaluronan-induced TSG-6 oligomers. *J. Biol. Chem.* **286**, 25675–25686 (2011).
- Migliorini, E. *et al.* Well-defined biomimetic surfaces to characterize glycosaminoglycan-mediated interactions on the molecular, supramolecular and cellular levels. *Biomaterials* **35**, 8903–8915 (2014).

26. Ratto, T. V. *et al.* Force spectroscopy of the double-tethered concanavalin-A mannose bond. *Biophys. J.* **86**, 2430–2437 (2004).
27. Eisele, N. B., Andersson, F. I., Frey, S. & Richter, R. P. Viscoelasticity of thin biomolecular films: a case study on nucleoporin phenylalanine-glycine repeats grafted to a histidine-tag capturing QCM-D sensor. *Biomacromolecules* **13**, 2322–2332 (2012).
28. Banerji, S. *et al.* Structures of the Cd44-hyaluronan complex provide insight into a fundamental carbohydrate-protein interaction. *Nat. Struct. Mol. Biol.* **14**, 234–239 (2007).
29. Teriete, P. *et al.* Structure of the regulatory hyaluronan binding domain in the inflammatory leukocyte homing receptor CD44. *Mol. Cell* **13**, 483–496 (2004).
30. Wolny, P. M. *et al.* Analysis of CD44-hyaluronan interactions in an artificial membrane system: insights into the distinct binding properties of high and low molecular weight hyaluronan. *J. Biol. Chem.* **285**, 30170–30180 (2010).
31. Banerji, S., Hide, B. R., James, J. R., Noble, M. E. & Jackson, D. G. Distinctive properties of the hyaluronan-binding domain in the lymphatic endothelial receptor Lyve-1 and their implications for receptor function. *J. Biol. Chem.* **285**, 10724–10735 (2010).
32. Eisele, N. B., Labokha, A. A., Frey, S., Gorlich, D. & Richter, R. P. Cohesiveness tunes assembly and morphology of FG nucleoporin domain meshworks - Implications for nuclear pore permeability. *Biophys. J.* **105**, 1860–1870 (2013).
33. Heinegard, D. & Hascall, V. C. Aggregation of cartilage proteoglycans. 3. Characteristics of the proteins isolated from trypsin digests of aggregates. *J. Biol. Chem.* **249**, 4250–4256 (1974).
34. Janshoff, A., Neitzert, M., Oberdorfer, Y. & Fuchs, H. Force Spectroscopy of Molecular Systems-Single Molecule Spectroscopy of Polymers and Biomolecules. *Angew. Chem. Int. Ed. Engl.* **39**, 3212–3237 (2000).
35. Fujii, T., Sun, Y. L., An, K. N. & Luo, Z. P. Mechanical properties of single hyaluronan molecules. *J. Biomech.* **35**, 527–531 (2002).
36. Bell, G. I. Models for the specific adhesion of cells to cells. *Science* **200**, 618–627 (1978).
37. Evans, E. & Ritchie, K. Dynamic strength of molecular adhesion bonds. *Biophys. J.* **72**, 1541–1555 (1997).
38. Merkel, R., Nassoy, P., Leung, A., Ritchie, K. & Evans, E. Energy landscapes of receptor-ligand bonds explored with dynamic force spectroscopy. *Nature* **397**, 50–53 (1999).
39. de Gennes, P. G. Polymers at an interface; a simplified view. *Adv. Colloid Interface Sci.* **27**, 189–209 (1987).
40. Chivers, C. E. *et al.* A streptavidin variant with slower biotin dissociation and increased mechanostability. *Nat. Methods* **7**, 391–393 (2010).
41. Neuert, G., Albrecht, C. H. & Gaub, H. E. Predicting the rupture probabilities of molecular bonds in series. *Biophys. J.* **93**, 1215–1223 (2007).
42. DeGrendele, H. C., Estess, P., Picker, L. J. & Siegelman, M. H. CD44 and its ligand hyaluronate mediate rolling under physiologic flow: a novel lymphocyte-endothelial cell primary adhesion pathway. *J. Exp. Med.* **183**, 1119–1130 (1996).
43. Ogino, S. *et al.* Two-state conformations in the hyaluronan-binding domain regulate CD44 adhesiveness under flow condition. *Structure* **18**, 649–656 (2010).
44. Martin, S. *et al.* Polymer hydrogel particles as biocompatible AFM probes to study CD44/hyaluronic acid interactions on cells. *Polymer* (2016) *In Press*.
45. Levesque, M. C. & Haynes, B. F. TNF α and IL-4 regulation of hyaluronan binding to monocyte CD44 involves posttranslational modification of CD44. *Cell. Immunol.* **193**, 209–218 (1999).
46. Jackson, D. G. Immunological functions of hyaluronan and its receptors in the lymphatics. *Immunol. Rev.* **230**, 216–231 (2009).
47. Jackson, D. G. Lymphatic Regulation of Cellular Trafficking. *J. Clin. Cell. Immunol.* **5**, 258–268 (2014).
48. Lawrance, W., Banerji, S., Day, A. J., Bhattacharjee, S. & Jackson, D. G. Binding of Hyaluronan to the Native Lymphatic Vessel Endothelial Receptor LYVE-1 Is Critically Dependent on Receptor Clustering and Hyaluronan Organization. *J. Biol. Chem.* **291**, 8014–8030 (2016).
49. Thakar, D. *et al.* A quartz crystal microbalance method to study the terminal functionalization of glycosaminoglycans. *Chem. Commun.* **50**, 15148–15151 (2014).
50. Yang, D., Ward, A., Halvorsen, K. & Wong, W. P. Multiplexed single-molecule force spectroscopy using a centrifuge. *Nat. Commun.* **7**, 11026 (2016).
51. Day, A. J. & Sheehan, J. K. Hyaluronan: polysaccharide chaos to protein organisation. *Curr. Opin. Struct. Biol.* **11**, 617–622 (2001).
52. Lesley, J. *et al.* TSG-6 modulates the interaction between hyaluronan and cell surface CD44. *J. Biol. Chem.* **279**, 25745–25754 (2004).
53. Beutel, O. *et al.* High-fidelity protein targeting into membrane lipid microdomains in living cells. *Angew. Chem. Int. Ed. Engl.* **53**, 1311–1315 (2014).
54. Lata, S., Gavutis, M., Tampe, R. & Piehler, J. Specific and stable fluorescence labeling of histidine-tagged proteins for dissecting multi-protein complex formation. *J. Am. Chem. Soc.* **128**, 2365–2372 (2006).
55. Lata, S., Gavutis, M. & Piehler, J. Monitoring the dynamics of ligand-receptor complexes on model membranes. *J. Am. Chem. Soc.* **128**, 6–7 (2006).
56. Eisele, N. B., Frey, S., Piehler, J., Gorlich, D. & Richter, R. P. Ultrathin nucleoporin phenylalanine-glycine repeat films and their interaction with nuclear transport receptors. *EMBO Rep.* **11**, 366–372 (2010).
57. Richter, R., Mukhopadhyay, A. & Brisson, A. Pathways of lipid vesicle deposition on solid surfaces: a combined QCM-D and AFM study. *Biophys. J.* **85**, 3035–3047 (2003).
58. Reviakine, I., Johannsmann, D. & Richter, R. P. Hearing what you cannot see and visualizing what you hear: interpreting quartz crystal microbalance data from solvated interfaces. *Anal. Chem.* **83**, 8838–8848 (2011).
59. Butt, H. J. & Jaschke, M. Calculation of thermal noise in atomic force microscopy. *Nanotechnology* **6**, 1–7 (1995).
60. Bustamante, C., Marko, J. F., Siggia, E. D. & Smith, S. Entropic elasticity of lambda-phage DNA. *Science* **265**, 1599–1600 (1994).

Acknowledgements

We thank M. Tammi (University of Eastern Finland, Kuopio, Finland) for providing the aggrecan G1 domain complex with cartilage link protein, J. Piehler and C. You (both University of Osnabrück, Germany) for providing tris-NTA-functionalized lipids, L. Yate (CIC biomaGUNE) for gold depositions, L. Bureau (University Grenoble Alpes) for fruitful discussions, and H. Davies (University Grenoble Alpes) for critical reading of the manuscript. This work was supported by the European Research Council (Starting Grant JELLY, No. 306435; to RPR) and the Spanish Ministry for Economy and Competitiveness (MAT2014-54867-R; to RPR). Additional support was also provided by the UK Medical Research Council to DGJ through MRC Human Immunology Unit Core funding.

Author Contributions

R.P.R. conceived the research; F.B., S.B., D.G.J. and R.P.R. designed the research; S.B., M.H. and D.G.J. contributed essential reagents; F.B. acquired data; F.B. and R.P.R. analyzed data, and wrote the paper, and D.G.J. and M.H. helped with editing. All authors commented on the manuscript.

Additional Information

Supplementary information accompanies this paper at <http://www.nature.com/srep>

Competing financial interests: M.H. is an inventor on patent US8759488 B2 describing traptavidin. All other authors declare no competing financial interests.

How to cite this article: Bano, F. *et al.* A single molecule assay to probe monovalent and multivalent bonds between hyaluronan and its key leukocyte receptor CD44 under force. *Sci. Rep.* **6**, 34176; doi: 10.1038/srep34176 (2016).



This work is licensed under a Creative Commons Attribution 4.0 International License. The images or other third party material in this article are included in the article's Creative Commons license, unless indicated otherwise in the credit line; if the material is not included under the Creative Commons license, users will need to obtain permission from the license holder to reproduce the material. To view a copy of this license, visit <http://creativecommons.org/licenses/by/4.0/>

© The Author(s) 2016

Supporting Information

A single molecule assay to probe monovalent and multivalent bonds between hyaluronan and its key leukocyte receptor CD44 under force

Fouzia Bano,¹ Suneale Banerji,² Mark Howarth,³ David G. Jackson,² Ralf P. Richter^{1,4,5,*}

¹CIC biomaGUNE, Paseo Miramon 182, 20009 Donostia-San Sebastian, Spain; ²MRC Human Immunology Unit, Weatherall Institute of Molecular Medicine, University of Oxford, Oxford, OX39DS, UK; ³Department of Biochemistry, University of Oxford, Oxford, OX13QU, UK;

⁴Université Grenoble Alpes - CNRS, Laboratoire Interdisciplinaire de Physique (LIPhy), BP 87, 38402 Saint Martin d'Hères, France; ⁵University of Leeds, School of Biomedical Sciences and School of Physics and Astronomy, Leeds, LS2 9JT, UK

*Corresponding author, email: rrichter@cicbiomagune.es

in working buffer. The complex contains multiple biotin moieties at random (uncontrolled) positions.

Quantification of CD44 surface density by spectroscopic ellipsometry (SE):

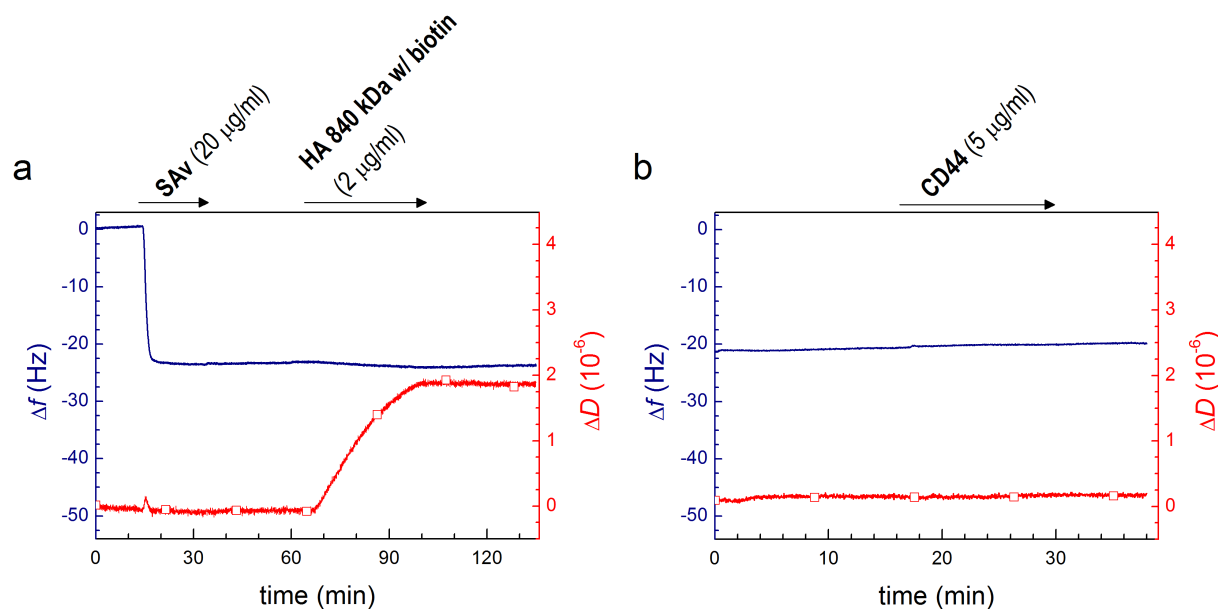
To estimate the surface density of CD44, the formation of CD44 monolayers was followed by SE. SE measurements were carried out at room temperature with a M2000V system (J. A. Woollam, Lincoln, NE, USA) and the data were analyzed using CompleteEASE software (J. A. Woollam) following established procedures.^{3,4} Briefly, gold-coated silicon wafers functionalized with biotinylated OEG monolayers were installed in a custom-built open cuvette (~180 μ l volume, passivated with 10 mg/ml bovine serum albumin for 20 min prior to use). The cuvette featured a magnetic stirrer which was used to homogenize the cuvette content for 20 s after injecting the sample into the cuvette and during rinses with working buffer; sample binding was followed in still solution. In the optical model to fit the data, the opaque gold film and the OEG monolayer were treated as a single isotropic layer and fitted as a B-Spline substrate, and the protein film made of SAV and CD44 was treated as an isotropic and transparent Cauchy layer. Areal protein mass densities were determined through de Feijter's equation,⁵ using a refractive index increment of 0.18 cm³/g.^{6,7}

AFM SMFS of SAV•biotin and TAV•biotin interactions:

Gold-coated AFM cantilevers were conditioned by exposure to UV/ozone for 30 min, and then immersed overnight at room temperature in a solution of linear OEG (7 units) with a hydroxyl and a thiol group at the ends (OEG thiol; Polypure) mixed with linear PEG (10 kDa) with a biotin and a thiol group at the ends (b-PEG thiol; IRIS biotech GmbH, Germany) in ultrapure water (total concentration 1 mM, molar ratio 4×10^4 OEG per 1 b-PEG). The substrates were then rinsed in ultrapure water, and immersed in working buffer for their final use.

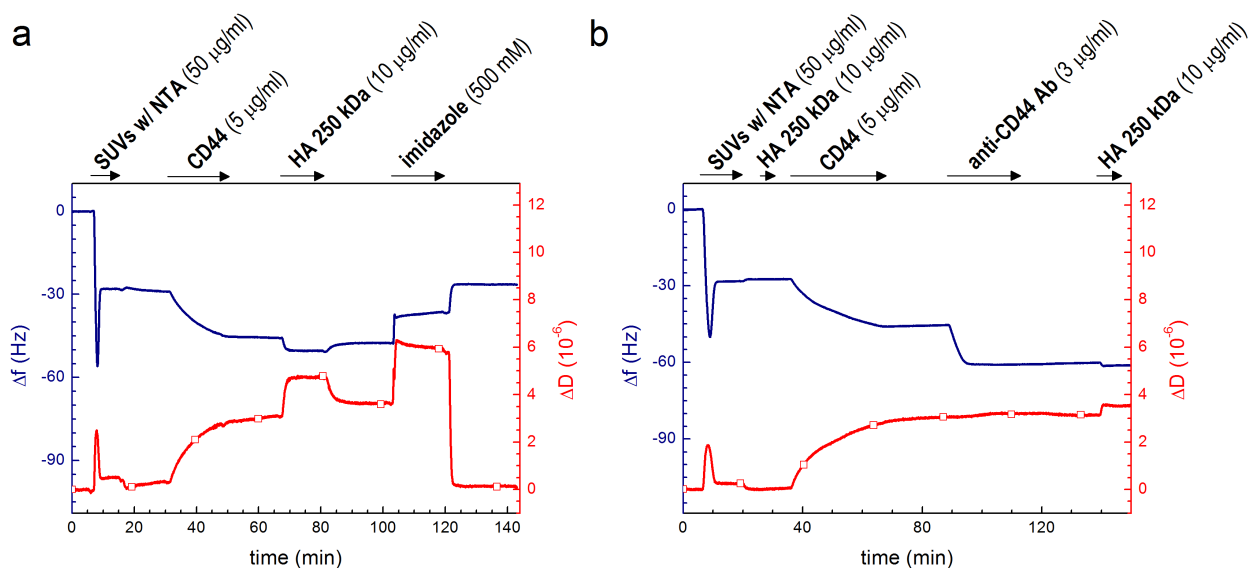
The mixed OEG/b-PEG monolayer thus formed displayed biotin at a dilution that showed a satisfactory binding frequency in AFM force spectroscopy on planar substrates displaying monolayers of SAV or TAV. Specifically, 65% of all force curves showed no specific unbinding event and 35% showed one event; two or more events were not observed. Monolayers of SAV and TAV were prepared and force data at various retract velocities acquired as described in the Methods section in the main text. Force curves were fit (JPK Data Processing Software) with a freely jointed chain (FJC) model, with the Kuhn segment length fixed to 0.7 nm (which describes the stretching of PEG chains in aqueous solution well over the force range relevant to our assays⁸) and the contour length as the only adjustable parameter. The effective spring constant k_{eff} , corresponding to the slope of the best-fit FJC model curve close to the rupture point, was used to compute the instantaneous loading rate $r = k_{\text{eff}}v$.

SUPPLEMENTARY FIGURES

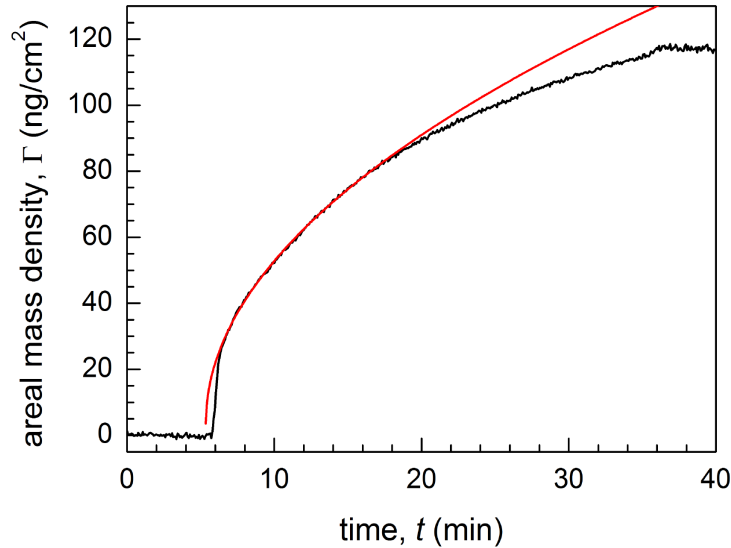


Supplementary Figure S1. QCM-D immobilization assays for end-biotinylated HA (840 kDa, 2.1 μm contour length) on biotinylated OEG monolayers, presented analogous to Fig. 1. The data in (a) confirm formation of a stable and dense SAV monolayer of about 4 nm thickness,^{9,10} and subsequent grafting of HA through biotin at the reducing end. The frequency decrease upon HA incubation was small ($\Delta f = -1.3 \pm 0.5$ Hz) and the concomitant dissipation shift large ($\Delta D = 3.1 \pm 0.2 \times 10^{-6}$), consistent with previously reported data, and reflecting the formation of a very soft and hydrated film.^{10,11} HA polymers lacking biotin do not bind to SAV monolayers, as shown previously.¹⁰ Data in (b) demonstrate that the CD44 construct employed in this study does not bind to a SAV monolayer that had previously been saturated with soluble biotin. Exposure to biotin does not induce a measurable QCM-D response due to biotin's small size (*cf.* Fig. S3b), and this trace is not shown here.

AFM probes were functionalized with HA as established through the QCM-D assay, but with a reduced HA incubation time of 6 min. At physiological ionic strength, an unperturbed HA chain of 2.1 μm contour length is expected to form a random coil with a radius of gyration of approximately 75 nm.¹² Considering the geometry of the AFM probe and cantilever, and assuming mass-transport limited binding of HA, we can estimate an upper limit of 24 ng/cm^2 for the HA surface coverage, corresponding to a root-mean-square distance between grafting points of 76 nm.¹³ This implies that the HA film is in the so-called 'mushroom regime', *i.e.* immobilized polymer coils barely interpenetrate and largely retain their random-coil conformation.¹⁴ Because of the sharpness of the AFM probe (the apex radius is typically 30 nm; *cf.* Fig. 1a) and the grafting density and conformation of HA, we expect only one or at most very few HA molecules to be able to contact the protein-covered surface.

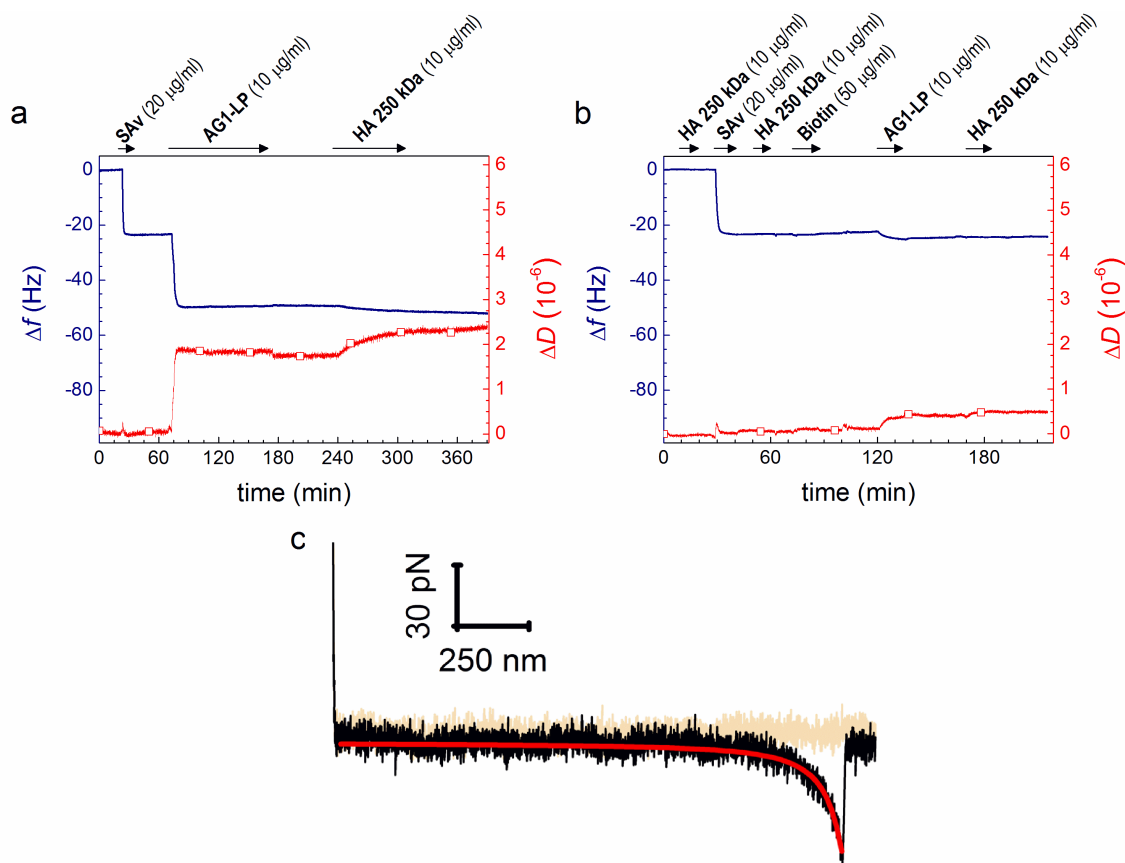


Supplementary Figure S2. QCM-D immobilization assays for CD44 on SLBs, presented analogous to Fig. 1. SLBs were formed by spreading of small unilamellar vesicles (SUVs) composed of a DOPC:(NTA)₃-SOA mixture (molar ratio 19:1); the two-phase responses in Δf and ΔD , the small final dissipation shift ($< 0.3 \times 10^{-6}$) and the final frequency shift (-29 ± 1 Hz) are characteristic for the formation of SLBs of good quality.^{4,15} QCM-D responses in (a) indicate the formation of a stable and HA-binding CD44 monolayer, and demonstrate that CD44 is specifically immobilized through its polyhistidine tag to the Ni²⁺-NTA moieties in the SLB (*i.e.* it can be fully eluted in imidazole). Frequency and dissipation shifts at about 120 min reflect the changes in the viscosity and density of the solution due to the presence of imidazole and are not due to surface effects. Data in (b) demonstrate that HA binds through the authentic HA-binding site on CD44 (largely blocked with anti-CD44 Ab).

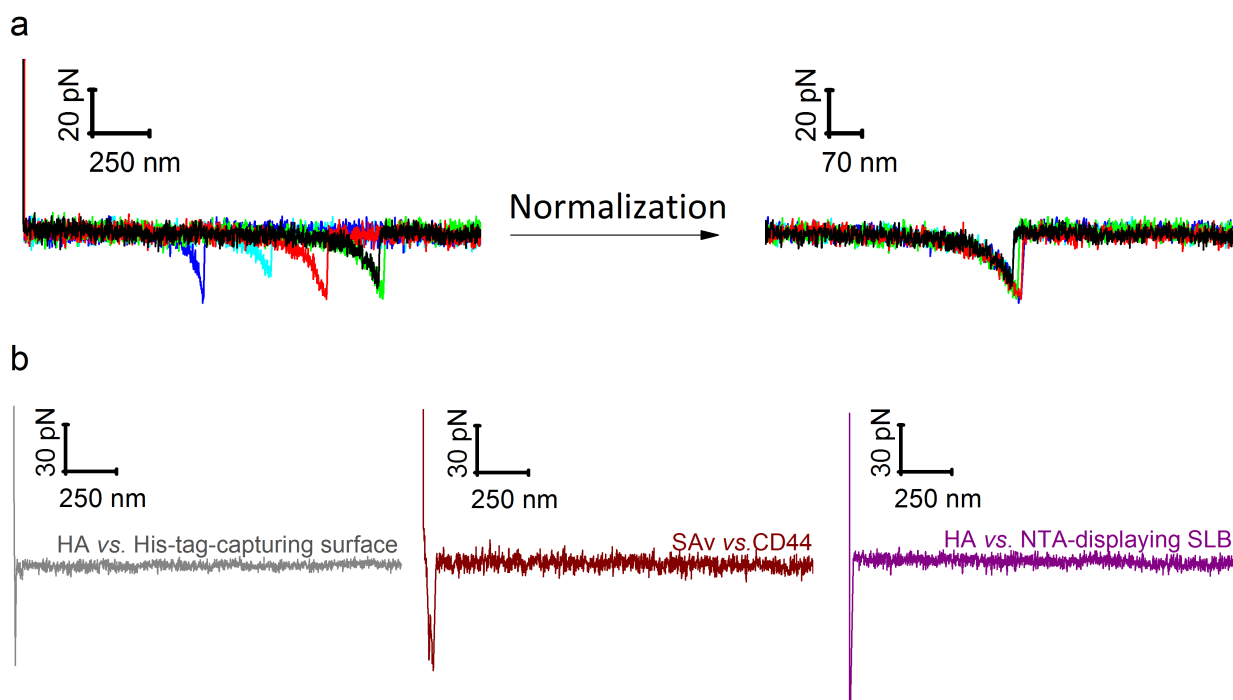


Supplementary Figure S3. Quantification of CD44 receptor density. Experimental data are shown in black, and the red curve is a best-fit theoretical curve for mass-transport limited binding. Immobilization of CD44 *via* its C-terminal biotin tag on a SAV-covered OEG monolayer (Supplementary Fig. S9a-c) was followed by SE to determine the areal protein mass density Γ (see Supplementary Methods for details). The incubation conditions were identical to those used for the preparation of ‘high receptor density’ samples for AFM force spectroscopy, *i.e.* 6.5 $\mu\text{g/ml}$ CD44 in still solution for 30 min (here from 6 to 36 min). At sufficiently low coverage, binding is expected to be mass-transport limited because the biotin•SAV bond forms fast. For mass-transport limited binding from still solution, binding is expected to scale with the square root of incubation time, with $\Gamma = 2c_b \sqrt{Dt/\pi}$, where c_b and D are the adsorbate’s concentration and diffusion constant in the bulk solution, respectively.¹⁶ This is indeed the case for CD44 up to $\Gamma \approx 80 \text{ ng/cm}^2$: the red curve corresponds to $\Gamma = \Gamma_0 + A\sqrt{(t - t_0)}$ with $A = 2c_b \sqrt{D/\pi} = 22.8 \pm 0.2 \text{ ng}/(\text{cm}^2 \text{min}^{1/2})$ and where the small offset $\Gamma_0 = 3.5 \pm 0.7 \text{ ng/cm}^2$ at $t_0 = 5.4 \pm 0.1 \text{ min}$ arises from the brief initial stirring required at the start of incubation for solution homogenization (errors represent confidence intervals from curve fitting). The progressive reduction in binding rate compared to the red curve at $\Gamma > 80 \text{ ng/cm}^2$ indicates that surface crowding limits binding at high surface coverage.

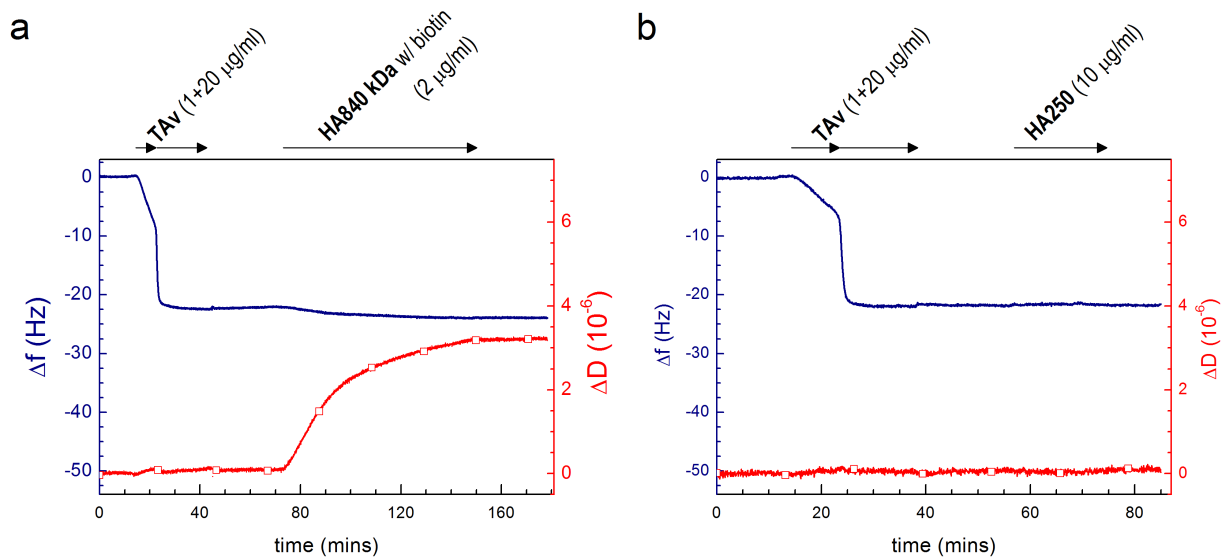
The surface coverage after 30 min of incubation was $110 \pm 5 \text{ ng/cm}^2$ (mean \pm variations around the mean from two independent measurements). From SDS PAGE analysis, we estimate the molecular weight of CD44 at 60 kDa, and ‘high receptor density’ surfaces thus correspond to a surface density of 1.8 pmol/cm^2 and an rms distance of 10 nm. The ‘low receptor density’ surfaces were obtained at 26-fold lower CD44 concentration (0.25 $\mu\text{g/ml}$) under otherwise identical incubation conditions. Based on the above equations we predict an areal mass density of 4.2 ng/cm^2 corresponding to a surface density of 0.07 pmol/cm^2 and an rms distance of 50 nm. We expect these estimates to be accurate also for CD44 anchorage *via* polyhistidine tags because binding rates are very similar (compare Fig. 2a with Supplementary Fig. S9a).



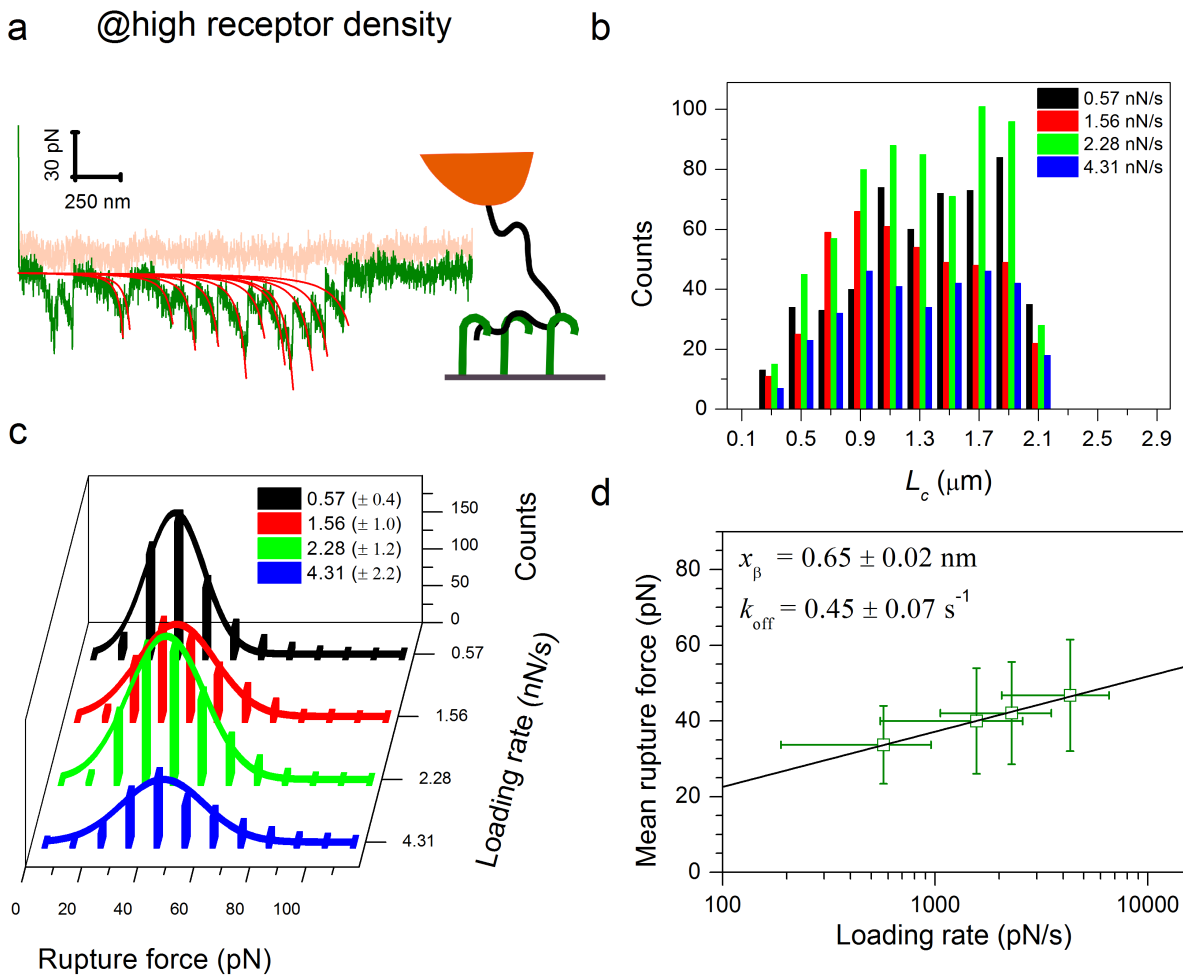
Supplementary Figure S4. Oriented protein immobilization is important for protein functionality. (a-b) QCM-D immobilization assay for a complex of aggrecan G1 domain and cartilage link protein (AG1-LP), presented analogous to Fig. 1. In contrast to CD44 and LYVE-1, AG1-LP was tagged using a procedure that is not site-specific; the tag was biotin and immobilization was performed as for HA (*cf.* Supplementary Fig. S1). Responses upon incubation of AG1-LP indicate stable and specific (*i.e.* largely blockable by saturation of SAV with free biotin) immobilization of the protein through biotin in a monolayer of 5 nm thickness. HA polymer bound stably and specifically to AG1-LP. Compared to CD44 (Fig. 2), the shifts in frequency (-1.7 ± 0.9 Hz) and dissipation ($0.5 \pm 0.2 \times 10^{-6}$) for HA-binding to AG1-LP were small even though AG1-LP is known to bind HA with high affinity.¹⁷⁻¹⁹ The reduced HA binding indicates that only a small fraction of the immobilized AG1-LP is active. Most likely, this is the consequence of tagging AG1-LP at random positions, leading to immobilization with an orientation that renders the HA-binding site of a large fraction of the AG1-LPs inaccessible. (c) Representative force-separation curve (pink – approach, black – retract; approach/retract velocity 1000 nm/s) recorded at maximal AG1-LP surface coverage. The curve shows a single rupture event. The red line is a best-fit WLC model curve with a persistence length of 4.1 nm characteristic for HA (*cf.* Fig. 3). This behavior was observed in 10% of the force curves; 88% showed no rupture event, and 2% showed two or more distinct rupture events. No rupture events (in $n = 200$ force curves per condition) were observed when either HA on the probe or AG1-LP on the surface were lacking, confirming that the observed interactions are specific. The frequency of binding events is remarkably small, if one considers that the employed HA polymers are long enough to bind about 100 AG1-LPs simultaneously, and that the polymer coil can readily explore a surface area containing tens of AG1-LPs. It is consistent with the limited activity of immobilized AG1-LP observed by QCM-D, and illustrates the importance of ensuring precise protein orientation.



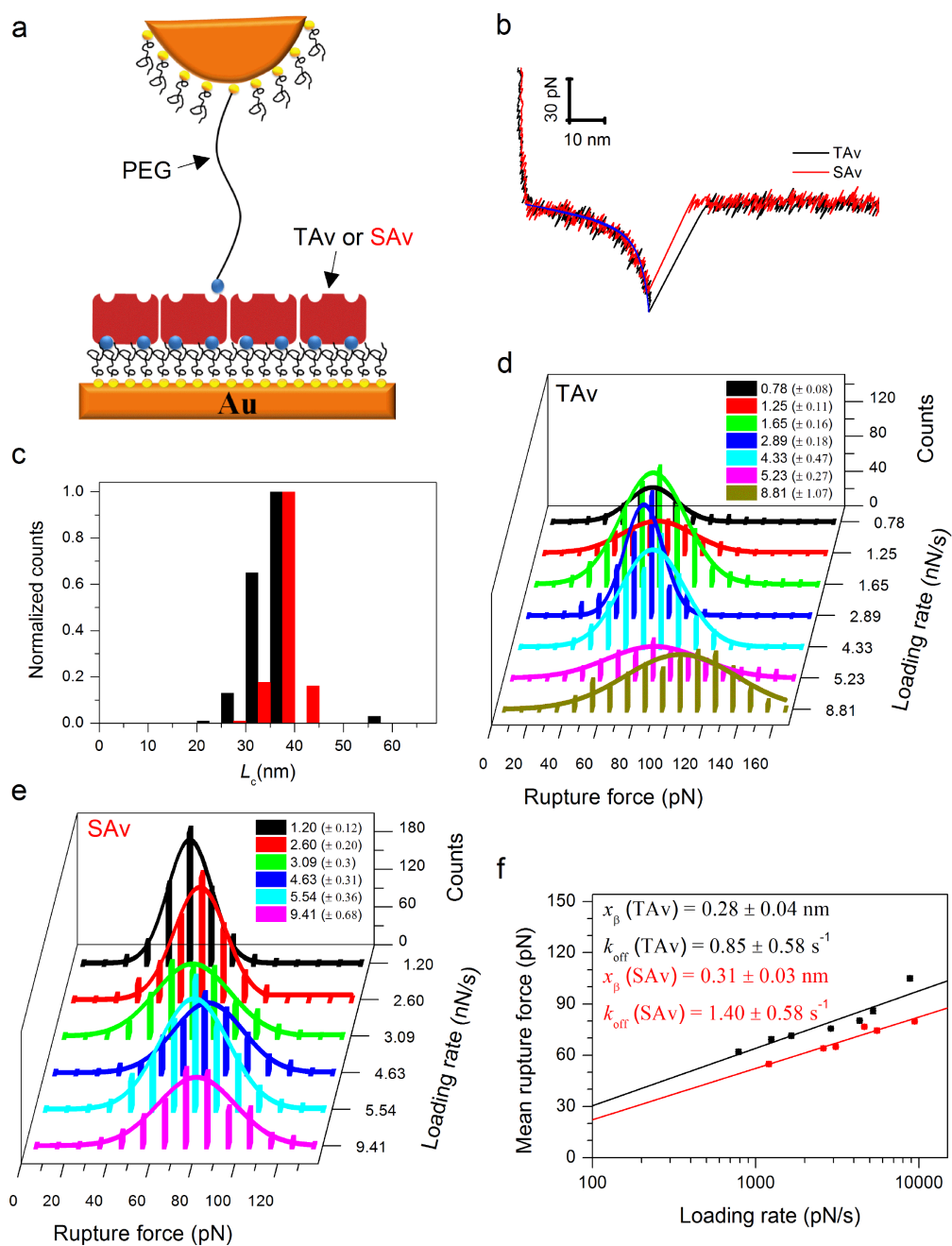
Supplementary Figure S5. Supplementary force spectroscopy data for HA•CD44 interactions. (a) Set of 5 randomly selected force-separation curves (retract velocity 1000 nm/s; conditions as in Fig. 3) featuring a single specific rupture event at various separation distances. The extension curves overlap when normalized,²⁰ confirming that interactions between a single HA chain and CD44 are probed. (b) Selected force-separation curves, registered at a retract velocity of 2000 nm/s, for control conditions as indicated. No specific rupture events are observed, and this feature is representative for all force curves acquired for the control conditions ($n = 200$ each).



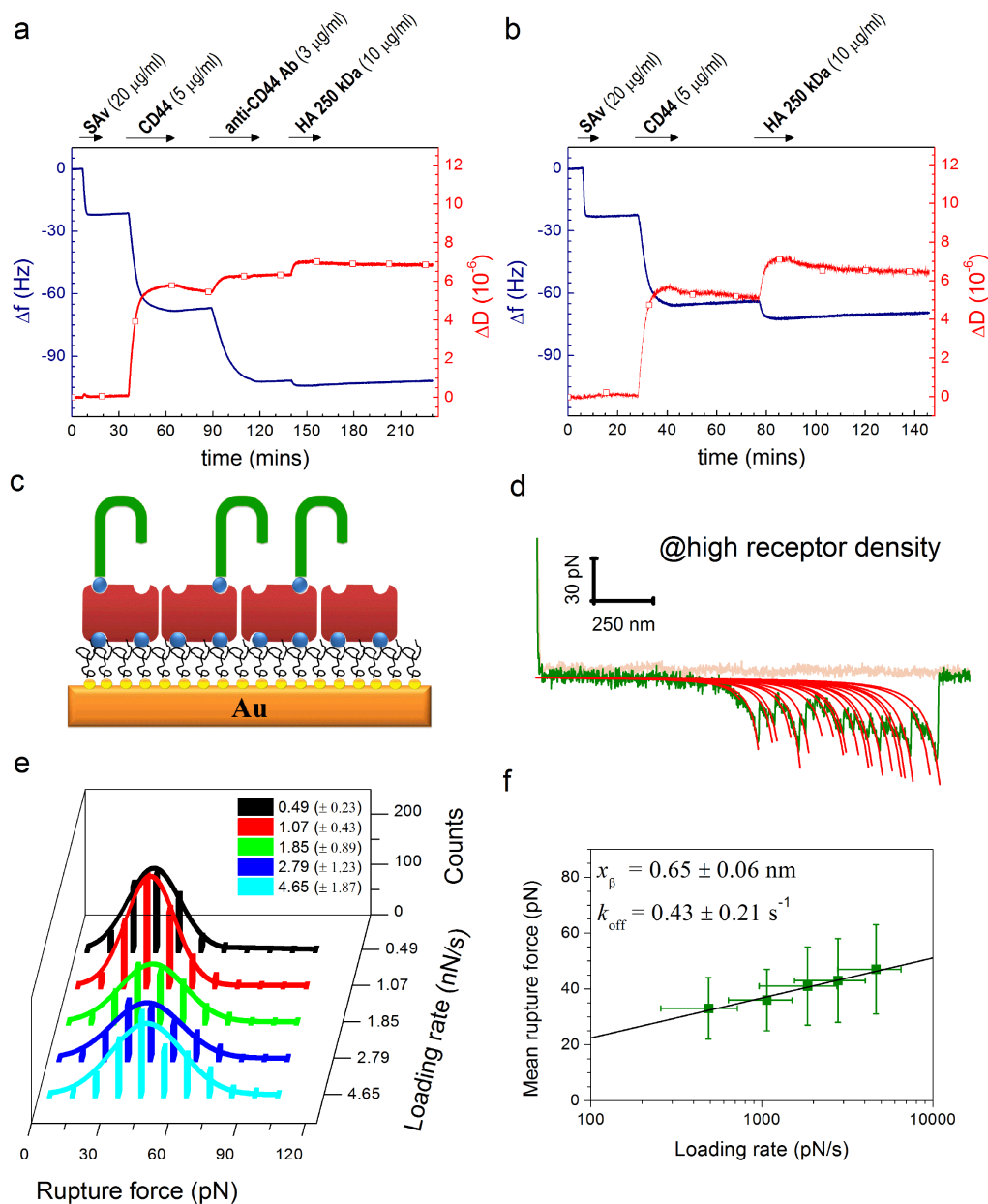
Supplementary Figure S6. QCM-D immobilization assays for biotinylated HA on TAV monolayers, presented analogous to Fig. 1. The QCM-D responses after TAV binding, and upon subsequent incubations with biotinylated HA (a) are virtually identical to those observed for SAV (*cf.* Supplementary Fig. S1a), confirming that the switch from SAV to TAV does not alter the surface density and organization of HA. The lack of binding for biotin-free HA (b) confirms specific immobilization through biotin. TAV was incubated sequentially at two distinct concentrations (first at 1 $\mu\text{g/mL}$ and then at 20 $\mu\text{g/mL}$) for technical reasons; this does not affect the properties of the final TAV monolayer.



Supplementary Figure S7. Immobilization of HA through TAV instead of SAV does not affect the CD44•HA force spectroscopy data. Force spectroscopy data shown here were obtained with HA immobilized *via* TAV and high CD44 surface density (rms inter-CD44-distance ~ 10 nm) on a His-tag-capturing sensor. (a) Representative force-separation curve (pink – approach, green – retract; approach/retract velocity 1000 nm/s). The red lines are best-fit WLC model curves ($L_p = 4.1$ nm fixed). Histograms of effective contour lengths (b) and rupture forces (c), and dynamic force spectra (d) are displayed analogous to Fig. 3c-e. Mean rupture forces and standard deviations are virtually identical to those obtained with HA immobilized *via* SAV (*cf.* Fig. 4d and Table 1).



Supplementary Figure S8. Biotin unbinds at larger forces from TAV than from SAV. (a) Schematic representation of the AFM SMFS assay (not to scale): biotin is attached through a PEG-thiol linker to a gold-coated AFM tip, and monolayers of TAV and SAV were formed as shown in Supplementary Figs. S6 and S1, respectively. (b) Representative force-separation curves (black – TAV, red – SAV; retract velocity 300 nm/s). The blue line is a best-fit FJC model curve (see Supplementary Methods for details). (c) Histograms of the effective contour length L_c of the b-PEG chain (black – TAV, red – SAV; retract velocity 300 nm/s). Rupture force histograms for TAV (d) and SAV (e) are displayed analogous to Fig. 3d. (f) Dynamic force spectra (black – TAV, red - SAV) obtained from the data in (d) and (e) and displayed analogous to Fig. 3e except for the error bars which here represent s.e.m, and these are essentially smaller than the symbol size. The data are in good agreement with previous reports by Chivers et al. (TAV•biotin: $x_\beta = 0.26 \pm 0.01$ nm, $k_{\text{off}} = 0.51 \pm 0.04$ s⁻¹; SAV•biotin: $x_\beta = 0.28 \pm 0.02$ nm, $k_{\text{off}} = 0.88 \pm 0.16$ s⁻¹).²¹



Supplementary Figure S9. Immobilization of CD44 through the biotin tag instead of the polyhistidine tag (both located at the C-terminus) does not affect the force spectroscopy data. (a-b) QCM-D immobilization assays, presented analogous to Fig. 1. QCM-D responses in (a) indicate formation of a stable and HA-binding CD44 monolayer on SA_v (see Supplementary Fig. S1b for a demonstration that binding is specific through biotin). Data in (b) demonstrate that HA binds through the authentic HA-binding site on CD44 (largely blocked with anti-CD44 Ab). (c) Representation of the surface architecture (not to scale) displaying CD44 anchored analogous to HA (*cf.* Fig. 1 and Supplementary Fig. S1) on a SA_v-coated biotinylated OEG monolayer. (d-f) Force spectroscopy data obtained at high CD44 surface density (CD44 was incubated at 6.5 $\mu\text{g/ml}$ for 30 min). (d) A representative force-separation curve (pink – approach, green – retract; retract velocity 2000 nm/s). The red lines are best-fit WLC model curves ($L_p = 4.1$ nm fixed). (e) Rupture force histograms displayed analogous to Fig. 3d. (f) Dynamic force spectra displayed analogous to Fig. 3e. Mean rupture forces and standard deviations are virtually identical to those obtained with CD44 immobilized through the polyhistidine tag (*cf.* Fig. 4d and Table 1).

SUPPORTING REFERENCES

- 1 Naldini, L., Blomer, U., Gally, P., Ory, D., Mulligan, R., Gage, F. H., Verma, I. M. & Trono, D. In vivo gene delivery and stable transduction of nondividing cells by a lentiviral vector. *Science* **272**, 263-267, (1996).
- 2 Tammi, R., Agren, U. M., Tuhkanen, A. L. & Tammi, M. Hyaluronan metabolism in skin. *Prog. Histochem. Cytochem.* **29**, 1-81, (1994).
- 3 Dubacheva, G. V., Curk, T., Mognetti, B. M., Auzely-Velty, R., Frenkel, D. & Richter, R. P. Superselective targeting using multivalent polymers. *J Am Chem Soc* **136**, 1722-1725, (2014).
- 4 Eisele, N. B., Frey, S., Piehler, J., Görlich, D. & Richter, R. P. Ultrathin nucleoporin phenylalanine–glycine repeat films and their interaction with nuclear transport receptors. *EMBO Rep.* **11**, 366-372, (2010).
- 5 De Feijter, J. A., Benjamins, J. & Veer, F. A. Ellipsometry as a tool to study the adsorption behavior of synthetic and biopolymers at the air–water interface. *Biopolymers* **17**, 1759-1772, (1978).
- 6 Richter, R. P., Rodenhausen, K. B., Eisele, N. B. & Schubert, M. in *Ellipsometry of Functional Organic Surfaces and Films* (eds Hinrichs, K. *et al.*) 223-248 (Springer 2014).
- 7 Zhao, H., Brown, P. H. & Schuck, P. On the distribution of protein refractive index increments. *Biophys J* **100**, 2309-2317, (2011).
- 8 Oosterhelt, F., Rief, M. & Gaub, H. E. Single molecule force spectroscopy by AFM indicates helical structure of poly(ethylene-glycol) in water. *New J. Phys.* **1**, 6, (1999).
- 9 Migliorini, E., Thakar, D., Sadir, R., Pleiner, T., Baleux, F., Lortat-Jacob, H., Coche-Guerente, L. & Richter, R. P. Well-defined biomimetic surfaces to characterize glycosaminoglycan-mediated interactions on the molecular, supramolecular and cellular levels. *Biomaterials* **35**, 8903-8915, (2014).
- 10 Baranova, N. S., Nileback, E., Haller, F. M., Briggs, D. C., Svedhem, S., Day, A. J. & Richter, R. P. The inflammation-associated protein TSG-6 cross-links hyaluronan via hyaluronan-induced TSG-6 oligomers. *J. Biol. Chem.* **286**, 25675-25686, (2011).
- 11 Richter, R. P., Hock, K. K., Burkhartsmeyer, J., Boehm, H., Bingen, P., Wang, G., Steinmetz, N. F., Evans, D. J. & Spatz, J. P. Membrane-grafted hyaluronan films: a well-defined model system of glycoconjugate cell coats. *J. Am. Chem. Soc.* **129**, 5306-5307, (2007).
- 12 Takahashi, R., Al-Assaf, S., Williams, P. A., Kubota, K., Okamoto, A. & Nishinari, K. Asymmetrical-flow field-flow fractionation with on-line multiangle light scattering detection. 1. Application to wormlike chain analysis of weakly stiff polymer chains. *Biomacromolecules* **4**, 404-409, (2003).
- 13 Goldstein, B., Coombs, D., He, X., Pineda, A. R. & Wofsy, C. The influence of transport on the kinetics of binding to surface receptors: application to cells and BIAcore. *J Mol Recognit* **12**, 293-299, (1999).
- 14 de Gennes, P. G. Polymers at an interface; a simplified view. *Adv. Colloid Interface Sci.* **27**, 189-209, (1987).
- 15 Richter, R. P., Berat, R. & Brisson, A. R. Formation of solid-supported lipid bilayers: an integrated view. *Langmuir* **22**, 3497-3505, (2006).
- 16 Hermens, W. T., Benes, M., Richter, R. & Speijer, H. Effects of flow on solute exchange between fluids and supported biosurfaces. *Biotechnol. Appl. Biochem.* **39**, 277-284, (2004).
- 17 Christner, J. E., Brown, M. L. & Dziewiatkowski, D. D. Affinity binding of the cartilage proteoglycan protein-keratan sulfate core to immobilized hyaluronic acid. *Anal Biochem* **90**, 22-32, (1978).

- 18 Tengblad, A. A comparative study of the binding of cartilage link protein and the hyaluronate-binding region of the cartilage proteoglycan to hyaluronate-substituted Sepharose gel. *Biochem. J.* **199**, 297-305, (1981).
- 19 Nieduszynski, I. A., Sheehan, J. K., Phelps, C. F., Hardingham, T. E. & Muir, H. Equilibrium-binding studies of pig laryngeal cartilage proteoglycans with hyaluronate oligosaccharide fractions. *Biochem. J.* **185**, 107-114, (1980).
- 20 Janshoff, A., Neitzert, M., Oberdorfer, Y. & Fuchs, H. Force Spectroscopy of Molecular Systems-Single Molecule Spectroscopy of Polymers and Biomolecules. *Angew. Chem. Int. Ed. Engl.* **39**, 3212-3237, (2000).
- 21 Chivers, C. E., Crozat, E., Chu, C., Moy, V. T., Sherratt, D. J. & Howarth, M. A streptavidin variant with slower biotin dissociation and increased mechanostability. *Nat. Methods* **7**, 391-393, (2010).